

Ozone Data Assimilation with GEOS-Chem: a Comparison Between 3D-Var, 4D-Var, and Suboptimal Kalman Filter Approaches

K. Singh¹, A. Sandu¹, K. W. Bowman², M. Parrington^{3,4}, D. B. A. Jones⁴, and M. Lee²

¹Department of Computer Science, Virginia Polytechnic Institute and State University, 2202 Kraft Drive, Blacksburg, VA 24060, USA

²Jet Propulsion Laboratory, 4800 Oak Grove Drive, Pasadena, CA 91109, USA

³School of GeoSciences, University of Edinburgh, Edinburgh, UK

⁴Department of Physics, University of Toronto, ON M5S 1A7, Canada

Correspondence to: Adrian Sandu (sandu@cs.vt.edu)

Abstract. Chemistry transport models determine the evolving chemical state of the atmosphere by solving the fundamental equations that govern physical and chemical transformations subject to initial conditions of the atmospheric state and surface boundary conditions, e.g., surface emissions. The development of data assimilation techniques synthesize model predictions with measurements in a rigorous mathematical framework that provides observational constraints on these conditions.

Two families of data assimilation methods are currently widely used: variational and Kalman filter (KF). The variational approach is based on control theory and formulates data assimilation as a minimization problem of a cost functional that measures the model-observations mismatch. The Kalman filter approach is rooted in statistical estimation theory and provides the analysis covariance together with the best state estimate. Suboptimal Kalman filters employ different approximations of the covariances in order to make the computations feasible with large models. Each family of methods has both merits and drawbacks.

This paper compares several data assimilation methods used for global chemical data assimilation. Specifically, we evaluate data assimilation approaches for improving estimates of the summertime global tropospheric ozone distribution in August 2006 based on ozone observations from the NASA Tropospheric Emission Spectrometer and the GEOS-Chem chemistry transport model. The resulting analyses are compared against independent ozonesonde measurements to assess the effectiveness of each assimilation method. All assimilation methods provide notable improvements over the free model simulations, which differ from the ozonesonde measurements by about 20% (below 200 hPa). Four dimensional variational data assimilation with window lengths between five days and two weeks is the most accurate method,

20 with mean differences between analysis profiles and ozonesonde measurements of 1-5%. Two sequential assimilation approaches (three dimensional variational and suboptimal KF), although derived from different theoretical considerations, provide similar ozone estimates, with relative differences of 5-10% between the analyses and ozonesonde measurements.

Adjoint sensitivity analysis techniques are used to explore the role of of uncertainties in ozone precursors
25 and their emissions on the distribution of tropospheric ozone. A novel technique is introduced that projects 3D-Variational increments back to an equivalent initial condition, which facilitates comparison with 4D variational techniques

1 Introduction

Understanding the distribution of tropospheric ozone is one of the principal scientific challenges in
30 global atmospheric chemistry, e.g., Jacob (1999). Ozone is an integral constituent of the troposphere that plays a significant role in determining the chemical and radiative state of the atmosphere. Ozone in the stratosphere absorbs UV radiation, which is harmful to human health. In the upper troposphere ozone is a greenhouse gas through absorption of upwelling long wave radiation. In the mid-troposphere ozone is a precursor to OH radicals which moderate pollution levels. At the surface ozone is a pollutant causing
35 respiratory problems and affecting crop yields.

Numerous studies have attempted to quantify the distribution of tropospheric ozone through chemical transport models. The findings from these studies vary significantly due to the strong variability in ozone lifetimes and uncertainties in determining the amount of ozone lost through dry deposition, entered through upper troposphere-stratosphere exchanges, or evolved due to chemical reactions of trace gas
40 and emission precursors. The ozone lifetime varies from a few minutes at the surface, to a few days in the lower troposphere, to months in the upper troposphere. In such situations, it is important to validate the accuracy of model predictions against observed state of the atmosphere. Studies of variations in tropospheric ozone have been conducted through ozonesonde measurements, surface measurements (Logan, 1994, 1999; Tarasick et al., 2005; Oltmans et al., 2006), and satellite observations (Munro et al.,
45 1998; Tellmann et al., 2004).

Chemical data assimilation is a process of optimally combining imperfect observations with imperfect model simulations to produce a better estimate of the chemical state of the atmosphere and its boundary conditions (Carmichael et al., 2008). Considerable experience with data assimilation has been accumulated in the field of numerical weather prediction (Daley, 1991; Courtier et al., 1998; Rabier et al., 2000; Kalnay,
50 2002; Navon, 2009). In this work we focus on atmospheric constituent data assimilation. Chemical data assimilation poses specific challenges related to the multiphysics nature of the system, the stiffness of chemical kinetic equations, the sparseness of chemical observations, and the uncertainty in the levels of

anthropogenic and natural pollutants emitted into the atmosphere. Throughout this paper we will refer to model results as model predictions or model forecasts even when a past period is simulated.

55 Previous studies have employed various approaches to assimilating observations of trace gases for improved tropospheric chemistry representations. Data assimilation has been used to improve initial conditions, boundary values (emissions), and has resulted in improved air quality forecasts. The basic concepts of the variational approach to chemical data assimilation, and the construction of adjoint chemical transport models are discussed in detail in Sandu et al. (2005a); Hakami et al. (2007); Henze et al. (2007);
60 Carmichael et al. (2008). Early work in chemical data assimilation using variational techniques has been reported in Khattatov et al. (2000); Elbern and Schmidt (2001). Since then there is a growing body of literature with applications of 3D-Var and 4D-Var chemical data assimilations. 3D-Var was first used by Derber et al. (1991); Parrish and Derber (1992) and later applied by most of the meteorological centers (Courtier et al., 1998; Cohn et al., 1998; Gauthier et al., 1999a). A study on ozone improvement using
65 3D-Var assimilation is presented in Bei et al. (2008). Adjustment of gas phase chemical tracer initial conditions has been studied in Chai et al. (2007); Sandu et al. (2005b); Tang et al. (2004); Zhang et al. (2008). Adjustment of pollutant emissions through 4D-Var chemical data assimilation has been discussed in Chai et al. (2009). Data assimilation studies involving particle measurements to improve aerosol fields have been discussed in Hakami et al. (2005); Sandu et al. (2005b); Henze et al. (2004, 2009). Suboptimal Kalman
70 filters have been employed successfully for chemical data assimilation (Khattatov et al., 2000; Menard et al., 2000; Lamarque et al., 2002; Liao et al., 2006; Segers et al., 2005; Clark et al., 2006; Pierce et al., 2007; Parrington et al., 2009). The use of the ensemble Kalman filter (EnKF) (Evensen, 1994) in chemical data assimilation has been studied in Constantinescu et al. (2007a,b,c).

Different approaches to data assimilation are rooted in different theories (control, statistical estimation),
75 have different implementation and computational costs, and yield different performance on large scale problems of practical interest. A discussion on relationship between optimality of variational data assimilation and Kalman filters is presented in Li and Navon (2001). Houtekamer (2005) compared the quality of background statistics in 3D-Var and EnKF using radiance observations from satellite, while, Laroche et al. (2005) compared the characteristics 3D-Var and 4D-Var introduced in the operational suite of the Canadian
80 Meteorological Center (CMC). Constantinescu et al. (2007c) and Wu et al. (2008) compare the performances of EnKF with 4D-Var for chemical transport models on a regional scale using ground-level ozone measurements, while, Geer et al. (2006) provides an intercomparison of tropospheric ozone estimates obtained through 3D-Var, 4D-Var, and Kalman filter assimilation systems for both chemical transport and global circulation models as part of the Assimilation of ENVISAT Data (ASSET) project. The comparison between
85 techniques in Wu et al. (2008) is done in the context of regional assimilation and using surface network data.

The Tropospheric Emission Spectrometer (TES) (Beer et al., 2001) is the first dedicated infrared instrument

from which information of the global and vertical distribution of tropospheric ozone can be retrieved. Parrington et al. (2009) reported assimilation of vertical profiles of ozone from TES into the GEOS-Chem using suboptimal Kalman filter while Pierce et al. (2009) used TES and OMI in conjunction with a simple univariate filtering approach to investigate the impact of distant sources on air quality in Dallas and Houston. We have developed 3D-Var and 4D-Var data assimilation capabilities for GEOS-Chem v7. The goal of this paper is to provide the first direct comparison of global tropospheric ozone distribution estimated through 3D-Var, 4D-Var and suboptimal KF assimilation systems showcasing the potential of TES profile retrievals. The assessment of analyses generated through different assimilation systems are on the similar lines of Geer et al. (2006); Parrington et al. (2009).

This paper is structured as follows: Section 2 provides the mathematical overview of how observations are integrated into the model in different data assimilation systems. Section 5.2 discusses the characteristics of background error covariance matrices used in this study. Section 3 provides a brief overview of the global chemical transport model (GEOS-Chem) and its adjoint development. A description of the TES instrument, its observation operator and profile retrieval formulation is provided in Section 4. Section 6 details the experimental settings, computational costs and assessment of tropospheric ozone estimates through different assimilation systems. Summary and points of future work are discussed in Section 7.

2 Chemical data assimilation

Variational methods solve the data assimilation problem in an optimal control framework (Sasaki, 1958; Le Dimet and Talagrand, 1986; Courtier and Talagrand, 1987; Lions, 1971). Specifically, they attempt to find the control variable values (e.g., initial conditions) by minimizing the discrepancy between the model forecast and observations subject to the governing dynamic equations. In contrast, statistical estimation methods (generically known as Kalman filters/smoothers) solve the data assimilation problem in a Bayesian framework by combining probability densities of errors from different sources (Khattatov et al., 2000; Menard et al., 2000; Lamarque et al., 2002; Segers et al., 2005; Clark et al., 2006; Pierce et al., 2007; Parrington et al., 2009; Constantinescu et al., 2007b,c). In the following discussion, for simplicity of presentation, we focus on discrete models (in time and space) where the initial conditions are the control variables.

Data assimilation provides best estimates of the state of the atmosphere by combining the following three sources of information.

1. The apriori, or background state \mathbf{x}^b represents the best estimate of the true state \mathbf{x}^t available before any measurements are taken. This estimate is assumed unbiased, and the random background (estimation) errors ε^b are typically assumed to have a normal probability density with a background

error covariance matrix \mathbf{B}

$$\boldsymbol{\varepsilon}^b = \mathbf{x}^b - \mathbf{x}^t \in \mathcal{N}(\mathbf{0}, \mathbf{B}). \quad (1)$$

2. The model encapsulates our knowledge about physical and chemical laws that govern the evolution of the system. The model evolves an initial state $\mathbf{x}_0 \in \mathbb{R}^n$ at the initial time t_0 to future state values $\mathbf{x}_i \in \mathbb{R}^n$ at future times t_i ,

$$\mathbf{x}_i = \mathcal{M}_{t_0 \rightarrow t_i}(\mathbf{x}_0). \quad (2)$$

The size of the state space in realistic chemical transport models is very large. For example, a GEOS-Chem simulation at the $2^\circ \times 2.5^\circ$ horizontal resolution has $n \in \mathcal{O}(10^8)$ variables.

3. Observations $\mathbf{y}_i \in \mathbb{R}^m$ of the state are taken at times t_i , $1 = 1, \dots, N$

$$\mathbf{y}_i = \mathcal{H}(\mathbf{x}_i) + \boldsymbol{\varepsilon}_i^{\text{obs}}. \quad (3)$$

120 The observation operator \mathcal{H} maps the state space onto the observation space. In many practical situations \mathcal{H} is a highly nonlinear mapping, e.g., satellite radiance operators.

The observations are characterized by measurement and representativeness errors $\boldsymbol{\varepsilon}_i^{\text{obs}}$. The observation errors at each time are assumed to be independent of background errors, and independent of the observation errors at other times. They are typically assumed to have a normal distribution with mean zero and covariance \mathbf{R}_i ,

$$\boldsymbol{\varepsilon}_i^{\text{obs}} \in \mathcal{N}(\mathbf{0}, \mathbf{R}_i). \quad (4)$$

Based on these three sources of information data assimilation computes the posterior estimate \mathbf{x}^a of the true state; \mathbf{x}^a is called the ‘‘analysis’’ state.

2.1 Three dimensional variational (3D-Var) data assimilation

In the 3D-Var data assimilation the observations (3) are considered successively at times t_1, \dots, t_N . The background state (i.e., the best state estimate at time t_i) is given by the model forecast, starting from the previous analysis (i.e., best estimate at time t_{i-1}):

$$\mathbf{x}_i^b = \mathcal{M}_{t_{i-1} \rightarrow t_i}(\mathbf{x}_{i-1}^a).$$

The discrepancy between the model state \mathbf{x}_i and observations at time t_i , together with the departure of the state from the model forecast \mathbf{x}_i^b , are measured by the 3D-Var cost function:

$$\mathcal{J}(\mathbf{x}_i) = \frac{1}{2} (\mathbf{x}_i - \mathbf{x}_i^b)^T \mathbf{B}_i^{-1} (\mathbf{x}_i - \mathbf{x}_i^b) + \frac{1}{2} (\mathcal{H}(\mathbf{x}_i) - \mathbf{y}_i)^T \mathbf{R}_i^{-1} (\mathcal{H}(\mathbf{x}_i) - \mathbf{y}_i) \quad (5)$$

While in principle a different background covariance matrix should be used at each time, in practice the same matrix is re-used throughout the assimilation window. The 3D-Var analysis is computed as the state

which minimizes (5)

$$\mathbf{x}_i^a = \operatorname{argmin} \mathcal{J}(\mathbf{x}_i). \quad (6)$$

Typically a gradient-based numerical optimization procedure is employed to solve (6). The gradient $\nabla \mathcal{J}$ of the cost function (5) is

$$\nabla \mathcal{J}(\mathbf{x}_i) = \mathbf{B}_i^{-1} (\mathbf{x}_i - \mathbf{x}_i^b) + \mathbf{H}_i^T \mathbf{R}_i^{-1} (\mathcal{H}(\mathbf{x}_i) - \mathbf{y}_i) \quad (7)$$

Note that the gradient requires to computation of the linearized observation operator $\mathbf{H}_i = \mathcal{H}'(\mathbf{x}_i)$ about the current state \mathbf{x}_i .

Preconditioning is often used to improve convergence of the numerical optimization problem (6). A change of variables is performed by shifting the state and scaling it with the square root of covariance:

$$\hat{\mathbf{x}}_i = \mathbf{B}_i^{1/2} (\mathbf{x}_i - \mathbf{x}_i^b), \quad (8)$$

and carrying out the optimization with the new variables $\hat{\mathbf{x}}_i$.

2.2 Four dimensional variational (4D-Var) data assimilation

In strongly-constrained 4D-Var data assimilation all observations (3) at all times t_1, \dots, t_N are simultaneously considered. The control parameters are the initial conditions \mathbf{x}_0 ; they uniquely determine the state of the system at all future times via the model equation (2).

The discrepancy between model predictions and observations at all future times t_1, \dots, t_N , together with the departure of the initial state from the background state, are measured by the 4D-Var cost function:

$$\mathcal{J}(\mathbf{x}_0) = \frac{1}{2} (\mathbf{x}_0 - \mathbf{x}_0^b)^T \mathbf{B}_0^{-1} (\mathbf{x}_0 - \mathbf{x}_0^b) + \frac{1}{2} \sum_{i=1}^N (\mathcal{H}(\mathbf{x}_i) - \mathbf{y}_i)^T \mathbf{R}_i^{-1} (\mathcal{H}(\mathbf{x}_i) - \mathbf{y}_i) \quad (9)$$

Note that the departure of the initial conditions from the background is weighted by the inverse background covariance matrix, \mathbf{B}^{-1} , while the differences between the model predictions $\mathbf{H}(\mathbf{x}_i)$ and observations \mathbf{y}_i are weighted by the inverse observation error covariances, \mathbf{R}_i^{-1} .

The 4D-Var analysis is computed as the initial condition which minimizes (9) subject to the model equation constraints (2)

$$\mathbf{x}_0^a = \operatorname{argmin} \mathcal{J}(\mathbf{x}_0) \quad \text{subject to (2)}. \quad (10)$$

The model (2) propagates the optimal initial condition (9) forward in time to provide the analysis at future times, $\mathbf{x}_i^a = \mathcal{M}_{t_0 \rightarrow t_i}(\mathbf{x}_0^a)$.

The optimization problem (10) is solved numerically using a gradient-based technique. The gradient of (9) reads

$$\nabla J(\mathbf{x}_0) = \mathbf{B}_0^{-1} (\mathbf{x}_0 - \mathbf{x}_0^b) + \sum_{i=1}^N \left(\frac{\partial \mathbf{x}_i}{\partial \mathbf{x}_0} \right)^T \mathbf{H}_i^T \mathbf{R}_i^{-1} (\mathcal{H}(\mathbf{x}_i) - \mathbf{y}_i) \quad (11)$$

The 4D-Var gradient requires not only the linearized observation operator \mathbf{H}_i , but also the transposed derivative of future states with respect to the initial conditions. The 4D-Var gradient can be obtained effectively by forcing the adjoint model with observation increments, and running it backwards in time.

2.3 Suboptimal Kalman filter

The suboptimal Kalman filter is a sequential data assimilation approach (Khattatov et al., 2000) in which corrections in the concentration state vector are performed as soon as observations become available. Similar to 3D-Var, for every observation time t_i , this technique starts with the model forecast state (\mathbf{x}_i^f) and provides an expected analysis state (\mathbf{x}_i^a) that reduces the discrepancy between the model forecast and the observations \mathbf{y}_i . The analysis state vector is obtained as

$$\mathbf{x}_i^a = \mathbf{x}_i^f + \mathbf{K}_i \left(\mathbf{y}_i - \mathcal{H}(\mathbf{x}_i^f) \right) \quad (12)$$

where \mathbf{K} is the Kalman gain matrix, \mathbf{H} is the observation operator defined in equation (3), and \mathbf{y} the vector of observations at a given time. The Kalman gain matrix is defined as

$$\mathbf{K}_i = \mathbf{P}_i^f \mathbf{H}^T \left(\mathbf{H}_i \mathbf{P}_i^f \mathbf{H}_i^T + \mathbf{R}_i \right)^{-1} \quad (13)$$

140 where \mathbf{P}_i^f is the forecast error covariance matrix, \mathbf{R}_i is the observation error covariance matrix (4), and $\mathbf{H}_i = \mathcal{H}'(\mathbf{x}_i^f)$ is the linearized observation operator about the forecast state. If a diagonal or block-diagonal approximation of the error covariance matrix \mathbf{P}^f is used in equation (13), the analysis state generated through equation (12) is suboptimal. A description on the structure of \mathbf{P}^f is provided in Section 5.2.

At each observation time, along with the analysis state, the analysis error covariance matrix \mathbf{P}_i^a is also calculated as

$$\mathbf{P}_i^a = (\mathbf{I} - \mathbf{K}_i \mathbf{H}_i) \mathbf{P}_i^f \quad (14)$$

145 where \mathbf{I} is the identity matrix. There are multiple ways in which this analysis covariance matrix is made available to the next observation window. A simple approach is to keep the analysis covariance equal to the background covariance for the entire assimilation period (Parrington et al., 2009). Here we build diagonal approximations to \mathbf{P}_{i+1}^f by transporting variances (diagonal entries in \mathbf{P}_i^a) as passive tracers following Menard et al. (2000).

3 GEOS-Chem

150 In this paper we specifically consider GEOS-Chem (<http://geos-chem.org>), a global three-dimensional chemical transport model (CTM) driven by assimilated meteorological fields from Goddard Earth Observing System(GEOS-4) at the NASA Global Modeling and Assimilation Office (GMAO). It is being widely

used by research groups world-wide for performing global atmospheric chemistry studies. The model along with comparison of model predictions with observations was first described in Bey et al. (2001).
 155 GEOS-Chem accounts in detail for emissions from both natural and anthropogenic sources, for gas phase chemistry, aerosol processes, long range transport of pollutants, troposphere-stratosphere exchanges, etc. Anthropogenic emissions are obtained from the Global Emissions Inventory Activity (GEIA) (Benkovitz et al., 1996) while lightning NO_x source emissions are estimated using Price and Rind (1992), based on deep convective cloud top heights provided with the GMAO meteorological fields. Biomass burning emis-
 160 sions are based on Duncan et al. (2003) while biofuel emissions are from Yevich and Logan (2003). The meteorological fields have a horizontal resolution of 1° along latitude and 1.25° along longitude with 55 vertical levels, and a temporal resolution of 6 hrs (3 hrs for surface fields). We use GEOS-Chem v7.2.3. Subsequent model releases and references can be found at <http://geos-chem.org>.

The GEOS-Chem Adjoint system (http://wiki.seas.harvard.edu/geos-chem/index.php/GEOS-Chem_Adjoint)
 165 has been developed through a joint effort of groups at Virginia Tech, University of Colorado, Caltech, Jet Propulsion Laboratory, and Harvard (Henze et al., 2007; Singh et al., 2009a,b; Eller et al., 2009). The system can perform adjoint sensitivity analyses and 4D-Var chemical data assimilation. Inverse modeling studies with GEOS-Chem-Adjoint are exemplified in Henze et al. (2009); Kopacz et al. (2007); Zhang et al. (2009).

4 Tropospheric Emission Spectrometer (TES) observations

170 TES (Beer et al., 2001), one of four science instruments aboard NASA's Aura satellite, measures top-of-the-atmosphere high resolution spectrally-resolved longwave radiation (<http://tes.jpl.nasa.gov>). Vertical profiles of chemical concentrations are inferred from these radiance measurements using an off-line inversion process (Bowman et al., 2006). In this work we assimilate the retrieved ozone vertical profiles. Figure 1 shows the location of TES profiles for two days. Only TES profiles between 60°S- 60°N are considered
 175 because of the lower poleward thermal contrast.

A-priori information about the vertical concentration profile of the species of interest is needed to solve the retrieval inverse problem (the prior information does not come from the measurement). Let $\mathbf{x}^{\text{prior}}$ be the prior vertical ozone concentration profile (in volume mixing ratio units), and let $\mathbf{z}^{\text{prior}} = \log \mathbf{x}^{\text{prior}}$. Let $\mathbf{z}^{\text{true}} (= \log \mathbf{x}^{\text{true}})$ be the "true" atmospheric profile.

The vertical ozone profile retrieval can be expressed according to the formula

$$\hat{\mathbf{z}} = \mathbf{z}^{\text{prior}} + \mathbf{A} \left(\mathbf{z}^{\text{true}} - \mathbf{z}^{\text{prior}} \right) + \mathbf{G} \eta, \quad \hat{\mathbf{x}} = \exp(\hat{\mathbf{z}}). \quad (15)$$

180 Here \mathbf{A} is the averaging kernel matrix, \mathbf{G} is the gain matrix, and η is the spectral measurement error (assumed to have mean zero and covariance \mathbf{S}_η). More details can be found in Bowman et al. (2002); Jones et al. (2003); Worden et al. (2004).

The corresponding TES observation operator 3 is linear with respect to the logarithm of the concentrations, but nonlinear with respect to the concentration profile:

$$\mathcal{H}(\mathbf{x}) = \mathbf{z}^{\text{prior}} + \mathbf{A} \left(\log(\mathbf{L}\mathbf{x}) - \mathbf{z}^{\text{prior}} \right) \quad (16)$$

where \mathbf{L} is an interpolation operator that transforms \mathbf{x} from the GEOS-Chem N -level vertical grid to the TES profile retrieval P -level grid.

For this reason several chemical data assimilation studies based on TES retrieved profiles (Jones et al., 2003; Bowman et al., 2006; Parrington et al., 2009) have opted to perform the suboptimal Kalman filtering step (12) in the logarithm of the concentrations:

$$\log \mathbf{x}^a = \log \mathbf{x}^f + \mathbf{K} \left(\hat{\mathbf{z}} - \mathcal{H}(\mathbf{x}^f) \right)$$

185 Here \mathbf{K} is the Kalman gain matrix, \mathcal{H} is the observation operator defined in equation (16), and $\hat{\mathbf{z}}$ is the
 ozone profile retrievals from TES as described in equation (15). The analysis state is calculated in natural
 logarithm of volume mixing ratio (log VMR) at each observation grid point since the TES profile retrievals
 are in log VMR. An exponential operator and a linear interpolation operator based on pressure is then
 applied to this logarithm of analysis state in succession to regain the actual analysis state in GEOS-Chem
 190 grid domain. The points which do not lie on the observation grid remain unaffected by the assimilation.

The observation operator \mathcal{H} that transforms higher resolution model state to the TES profile vertical grid
 (observation grid) domain is expressed by equation (16). The Kalman gain matrix \mathbf{K} is defined by equation
 (13), particularized to the case where the state is the logarithm of volume mixing ratio.

For variational data assimilation the forcing calculation is carried out in concentrations. For this reason, an
 adjoint of the observation operator needs to be derived to update the gradients as described in equations
 (7) and (11)

$$\mathbf{H}^T \cdot \mathbf{v} = \left(\frac{\partial}{\partial \mathbf{x}} (\mathbf{A} \log(\mathbf{L}\mathbf{x})) \right)^T \cdot \mathbf{v} = \mathbf{L}^T \cdot \begin{pmatrix} (\mathbf{L}\mathbf{x})_0^{-1} & 0 & \cdots & 0 \\ 0 & (\mathbf{L}\mathbf{x})_1^{-1} & \cdots & 0 \\ \vdots & \vdots & \ddots & \vdots \\ 0 & 0 & \cdots & (\mathbf{L}\mathbf{x})_P^{-1} \end{pmatrix} \cdot \mathbf{A}^T \cdot \mathbf{v}$$

Here, $\mathbf{H} = \mathcal{H}'(\mathbf{x})$ is a matrix and $\mathbf{v} = \mathbf{R}^{-1}(\mathcal{H}(\mathbf{x}) - \mathbf{y})$. The TES averaging kernel \mathbf{A} is usually a non-
 195 symmetric matrix, and the result of $\mathbf{A}^T \cdot \mathbf{v}$ is fed to the interpolation operator to construct the diagonal
 matrix with the i -th element being $1/(\mathbf{L}\mathbf{x})_i$. The term \mathbf{L}^T is the adjoint of the interpolation operator and
 brings entities from the TES profile retrieval domain back to the GEOS-Chem model domain.

Note that the TES data can be biased by as much as 10% (Nassar et al., 2008). We have estimated the bias
 using the technique proposed in Nassar et al. (2008) and have removed it before assimilating the data.

200 5 Experimental setting for data assimilation

For numerical experiments, we employ GEOS-Chem v7-04-10 adjoint code package (Singh et al., 2009b), capable of performing both 3D-Var and 4D-Var data assimilations with real data. It also incorporates sub-optimal Kalman filter approach of data assimilation developed in Parrington et al. (2009). We assimilate Tropospheric Emission Spectrometer (TES) satellite ozone profile retrievals into the GEOS-Chem model
205 and validate the generated analyses against an independent observation dataset provided by direct ozone profile measurements from ozonesondes. The numerical optimization method used in all variational experiments is the limited memory bound-constrained BFGS (Zhu et al., 1997). This quasi-Newton approach has become the “gold standard” in solving large scale chemical data assimilation problems (Sandu et al., 2005a).

210 Simulations with GEOS-Chem v7 adjoint can be carried out at $4^\circ \times 5^\circ$ and $2^\circ \times 2.5^\circ$ resolutions. We have used $4^\circ \times 5^\circ$ resolution in all our experiments. There are 46×72 latitude-longitude grid boxes at this resolution, and 55 vertical levels; near the equator and at ground level each grid box covers an area of about $400 \text{ km} \times 500 \text{ km}$. The model has been modified to use the linearized ozone (linoz) scheme (McLinden et al., 2000) for a better estimation of ozone exchanges at troposphere-stratosphere boundary.
215 This scheme is available in v8 and above (see <http://geos-chem.org>). We performed data assimilation for only the first 23 model levels (for up to about 50 hPa), which encompasses where TES observations are most sensitive.

5.1 Data assimilation schemes

The 3D-Var data assimilation experiments were performed for a period of two weeks in the month of
220 August 2006, starting at 00:00(GMT) on August 1st. The TES data was read once every four simulation hours; the observation operator called at model time t (hours) reads in all the measurements collected within the interval $t - 2$ (hours) to $t + 2$ (hours). 3D-Var data assimilation treats all observations in this interval as instantaneous, and assimilates them in the same optimization run. In all our 3D-Var experiments, we performed 8 iterations per analysis since the cost function decreased significantly within the first few
225 iterations. It is important to note that 3D-Var does not involve any model adjoint calculations; gradients require only the adjoint of the observation operator. The optimization adjusts ozone concentrations. The generated analysis profile at the end of each observation window is evolved through the forward model that becomes the initial condition for the next observation window. It is also important to mention here that a new background error covariance matrix (17) is constructed for every observation window.

230 The setup for data assimilation using the suboptimal Kalman filter is quite similar to 3D-Var where we assimilated TES profile retrievals into GEOS-Chem over a two week period from 00:00 GMT on August 1, 2006 to 00:00 GMT on August 15, 2006. Observations were read every 4 hours and analysis states were

generated for each observation window through the sequential update formula (12).

The 4D-Var data assimilation experiments were performed for two different assimilation window lengths
 235 to adjudge if model errors hamper the quality of assimilations in GEOS-Chem involving longer assimila-
 tion windows; 4D-Var is strongly constrained by the forward model equation (10). Starting at 00:00 GMT
 on August 1, 2006, the first assimilation window is considered to be of five days while the second window
 is of two weeks. All the three assimilation systems had the same initial conditions to start with and were
 generated through a free GEOS-Chem model run. There were 12 optimization iterations performed in
 240 order to improve the ozone initial condition. Each iteration during 4D-Var assimilation includes a forward
 model and a backward model adjoint run. TES profile retrievals were read every 4 hours during the model
 adjoint run, and the cost function and adjoint gradients accumulated the impact of all 4 hour data sets
 throughout the assimilation window. Contrary to 3D-Var and suboptimal KF, where analysis states are
 generated sequentially every observation window, in 4D-Var the analysis is generated only at the initial
 245 time and accounts for the mismatch between observations and model predictions over all the observations
 in the assimilation window.

5.2 Specification of error variances

We consider a diagonal background error covariance matrix (\mathbf{B}) in all our variational data assimilation
 experiments for simplicity. The initial variances (the diagonal entries of the \mathbf{B} matrix) are constructed
 from the average background concentrations \mathbf{x}_0^B on each of the Nlev model vertical layers

$$\mathbf{B} = \begin{bmatrix} \mathbf{B}^{(0)} & 0 \dots & 0 \\ 0 & \mathbf{B}^{(1)} \dots & 0 \\ \vdots & \ddots & \vdots \\ 0 & 0 \dots & \mathbf{B}^{(\text{Nlev})} \end{bmatrix} \quad (17)$$

where

$$\mathbf{B}^{(\ell)} = \begin{bmatrix} \sigma_\ell^2 & 0 \dots & 0 \\ 0 & \sigma_\ell^2 \dots & 0 \\ \vdots & \ddots & \vdots \\ 0 & 0 \dots & \sigma_\ell^2 \end{bmatrix}_{\text{dim} \times \text{dim}}, \quad \text{dim} = \text{Nlon} \cdot \text{Nlat}, \quad (18)$$

with

$$\sigma_\ell = \frac{\alpha_{\text{rel}}}{\text{dim}} \sum_{i=1}^{\text{Nlon}} \sum_{j=1}^{\text{Nlat}} \mathbf{x}_0^B(i, j, \ell, s_{O_3}), \quad \ell = 1, \dots, \text{Nlev}, \quad s_{O_3} = \text{index of ozone}. \quad (19)$$

The relative uncertainty level in the background initial conditions (i.e., at the beginning of the assimilation
 window) is taken to be 50%, i.e., $\alpha_{\text{rel}} = 0.5$.

The forecast error covariance matrix \mathbf{P}^f used in our suboptimal Kalman filter approach is diagonal. The

initial forecast error is assumed to be 50% of the initial forecast field that is supposed to capture the representativeness error as well. In matrix form, \mathbf{P}_0^f is represented as

$$\mathbf{P}_0^f = \begin{bmatrix} \mathbf{P}_0^{f(0)} & 0 \dots & 0 \\ 0 & \mathbf{P}_0^{f(1)} & \dots & 0 \\ \vdots & \ddots & & \vdots \\ 0 & 0 \dots & \mathbf{P}_0^{f(\text{Nobs})} \end{bmatrix} \quad (20)$$

where Nobs is the number of observation points (in our case, the number of grid points in the TES retrieval domain). The initial forecast error covariance matrix block corresponding to each observation grid point is given as

$$\mathbf{P}_0^{f(i)} = \alpha_{\text{rel}} \cdot \begin{bmatrix} \mathbf{x}_0^f(i,1,s_{O3}) & 0 & \dots & 0 \\ 0 & \mathbf{x}_0^f(i,2,s_{O3}) & \dots & 0 \\ \vdots & \ddots & & \vdots \\ 0 & 0 & \dots & \mathbf{x}_0^f(i,\text{Nret},s_{O3}) \end{bmatrix}_{\text{Nret} \times \text{Nret}}, \quad i = 1, 2, \dots, \text{Nobs}, \quad (21)$$

250 where Nret is the number of vertical TES profile retrieval levels. Although the initial forecast error covariance matrix \mathbf{P}^f and all analysis \mathbf{P}^a 's henceforth are diagonal and there are no horizontal correlations being accounted for, the averaging kernels in the observation operator of TES as defined in equation (16) provide vertical correlations when operated on \mathbf{P}^f through equation (13). A detailed discussion on how to efficiently extend the background error covariance matrices to non-diagonal forms that capture spatial
255 error correlations is provided in Singh et al. (2010a).

6 Data assimilation results

6.1 Computational costs

The 3D-Var and suboptimal KF frameworks are built on top of GEOS-Chem v7 package which uses Sparse Matrix Vectorized GEAR (SMVGEAR) solver for chemistry. However, to construct the adjoint of chemistry
260 required by the 4D-Var, we implemented the Kinetic PreProcessor (KPP) solver (Damian et al., 2002) into GEOS-Chem which not only provides a suite of high performance chemical solvers to choose from but also generates automatically the continuous and discrete adjoint codes (Daescu, 2000, 2003; Sandu et al., 2003a,b). A detailed discussion on interfacing KPP with GEOS-Chem and comparison with native SMVGEAR solver for accuracy and computational performance is presented in Eller et al. (2009). As
265 pointed out in Henze et al. (2007), the computational cost of Rosenbrock solver increases significantly with the tolerance levels; higher tolerances use smaller internal time steps requiring more computation. In our experiments, we have set $\text{RTOL}=10^{-3}$ and $\text{ATOL}=10^{-2}$ to achieve moderate to high accuracy.

The suboptimal Kalman filter is less expensive than 3D-Var since it generates the analysis through the single update formula (12), while 3D-Var requires a few iterations before the optimization routine could generate a stable optimal analysis field. This is true however as long as the forecast error covariance matrix is diagonal. Once we move to non-diagonal matrices, the cost of calculating Kalman gain matrix (13) can be high, although this can be parameterized following, for example, Khattatov et al. (2000). In the case of 3D-Var and 4D-Var, using even full \mathbf{B} matrix adds a minimal cost to the overall simulation since the complete matrix is never constructed; at each step only a matrix vector product is required and efficient techniques are employed to derive the inverse and other powers of \mathbf{B} matrix (Singh et al., 2010a). The 4D-Var assimilation is the most expensive of all the assimilation systems under consideration. The reason is attributed to the fact that a single 4D-Var iteration performs both the forward and adjoint model runs, where, several variables on which the adjoint equation depends on, are written in checkpoint files in the forward model run.

Table 1 provides a comparison of the computational costs of the different data assimilation systems and the cost of free running model for a 24 hour simulation. All the simulations are performed on a Dell Precision T5400 workstation with two quad-core Intel(R) Xeon(R) processors, with clock speed 2.33GHz, and 16GB of RAM shared between the two processors.

Table 1. Timing results for GEOS-Chem free model runs using SMVGEAR and KPP chemistry, suboptimal Kalman filter, 3D-Var and 4D-Var data assimilations with diagonal background error covariance matrix for a 24 hour simulation starting 00:00 GMT August 1, 2006.

Experiment Description	CPU Time
Free model run, SMVGEAR chemistry solver	2 min 50 sec
Free model run, KPP chemistry solver	3 min 18 sec
Suboptimal Kalman filter with diagonal \mathbf{P}^f	3 min 08 sec
3D-Var with diagonal \mathbf{B}	3 min 57 sec
4D-Var with diagonal \mathbf{B} (per model run)	16 min 51 sec

6.2 Comparison with ozonesonde measurements

In order to assess the quality of analysis fields generated through different assimilation systems, we use ozonesonde profiles measured by the INTEX Ozonesonde Network Study 2006 (IONS-6) (<http://croc.gsfc.nasa.gov/intexb/ions06.html>) (Thompson et al., 2007a, 2007b)) for the month of August, assuming that these measurements provide values close to the true state of the atmosphere. There are 418 ozonesondes launched from 22 stations across North America as shown in the Figure 1. A detailed description of the number of ozonesondes launched per station with longitude and latitude information can be found in Parrington et al. (2008). The ozonesonde observations are not used in data assimilation, and therefore pro-

vide an independent data set against which the analysis results are validated. Forecast scoring techniques using assimilated data as described in Wu et al. (2008); Constantinescu et al. (2007c) do not provide a fair assessment of the quality of assimilation for sparse spatio-temporal sampling and longer time scales used
 295 in this analysis.

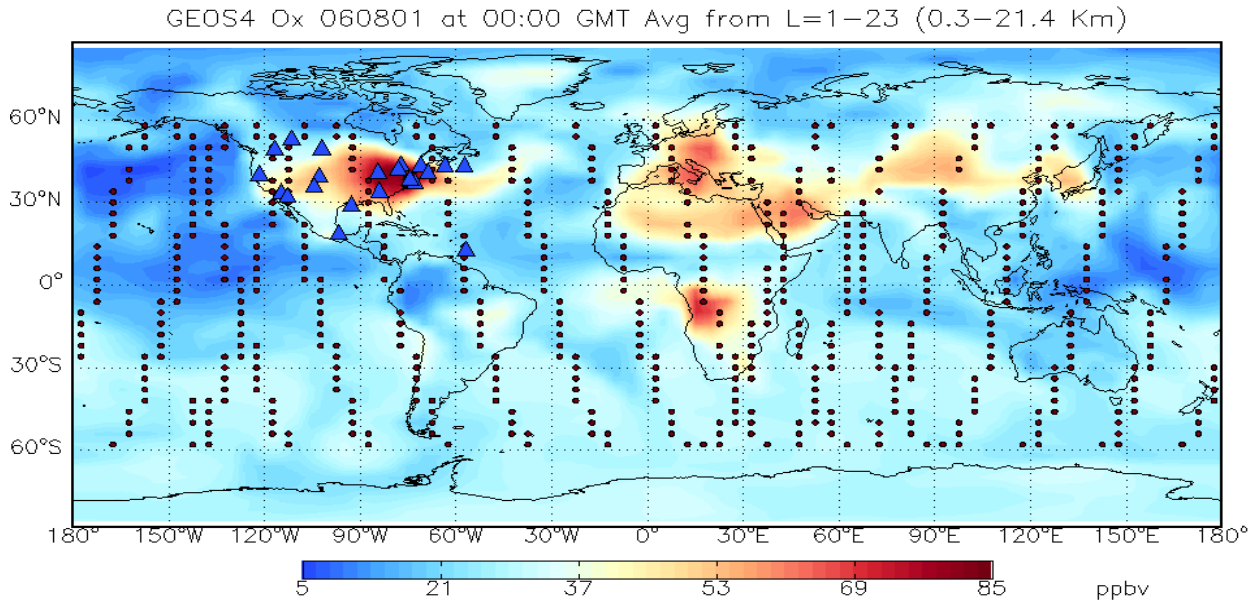


Fig. 1. Ozonesonde sounding stations (triangles) used during IONS06 campaign and AURA/TES satellite trajectory snapshots (dots) plotted over the global ozone distribution on August 1st, 2006.

We first consider the case where the assimilation window length is five days. As per the property of sequential data assimilation algorithms, the model forecast is corrected as soon as an observation is available. Ingesting observations every four simulation hours, we obtain an analysis field every four hours that accounts for the mismatch between the model prediction and the observations within that observation
 300 window. However, it is important to note that the model prediction at any observation window incorporates implicitly the corrections from all previous observations. Thus, as we move forward in time, the analysis field agrees better with the true state of the atmosphere. 4D-Var on the other hand accumulates the forcing due to mismatch between model forecast and observations throughout the assimilation window to produce an initial condition that, when evolved forward in time through the model, will best fit
 305 the observations. Therefore, in the case of sequential assimilation approaches, to obtain a stable analysis state that resembles the true chemical state of the atmosphere at a particular instant, we need to start the simulation days or months prior to that instant to benefit from earlier observations. 4D-Var is advantageous in situations where past observations are not available, as it provides the best estimate using only the observations available in the assimilation window under consideration.

310 We present in Figure 2, a comparison of analysis profiles obtained from different assimilation systems, and free GEOS-Chem model run against ozonesonde measurement data. The left panel shows vertical ozone profiles (concentrations against pressure levels); the model predictions are sampled at the locations and times of ozonesonde measurements available in the 5-day assimilation window. The differences between model results and ozonesonde data reflect model prediction errors; one error vertical profile is obtained for each ozonesonde launch. The center and right panels show the mean and the standard deviation of these errors. The plots provide an assessment of the quality of tropospheric ozone estimates given by the free model run, and by data assimilation systems based on suboptimal Kalman filter, 3D-Var and 4D-Var approaches. The errors also reflect the impact of TES profile retrievals on these assimilation systems.

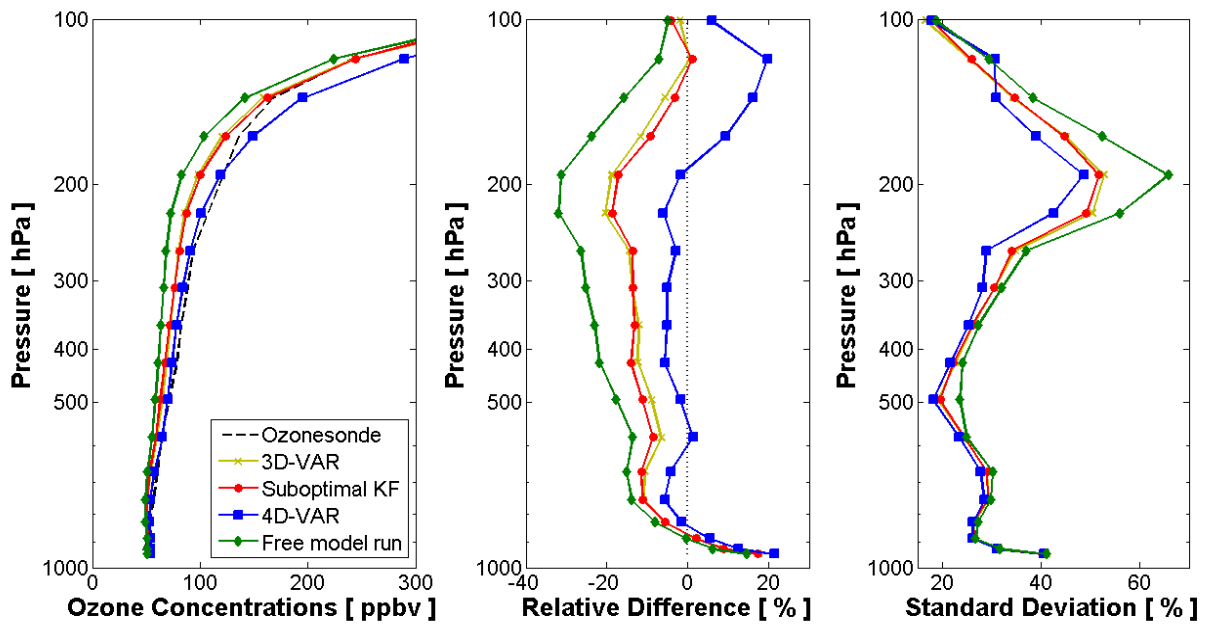


Fig. 2. The impact of ozone profile retrievals from TES on data assimilation systems for GEOS-Chem. Left panel: mean ozone concentrations sampled at ozonesonde locations and times for 3D-Var, 4D-Var, suboptimal KF analyses and free model trajectories. Center panel: relative mean errors of predicted ozone concentrations with respect to ozonesonde measurements. Right panel: standard deviation of absolute values of errors with respect to ozonesonde measurements. The data is averaged over all ozonesonde launches. These plots were generated from 5 days simulation from 00:00 GMT August 1, 2006 to 00:00 GMT August 6, 2006 and compared against ozonesonde data available for the month of August.

It is evident from the plots in Figure 2 that 4D-Var provided the best estimate for lower and mid troposphere ozone concentrations. The relative difference between the mean ozone analysis field and the ozonesonde measurements were decreased to less than 4% up to 180 hPa as compared to 5-20% in cases of suboptimal KF and 3D-Var. The overestimate of ozone in the upper troposphere is likely due to the

accumulated impact of the TES bias. The bias correction approach described in Nassar et al. (2008) may not be sufficient for assimilation studies and suggests an on-line bias correction scheme may be needed in the future. There was also a substantial improvement in the variance of the assimilation relative to the ozonesonde measurements, particularly for the 4D-Var case at 200 hPa. Consequently, the satellite observations have an impact not only on the mean value of tropospheric ozone but are also providing some additional information on the ozone distribution. A detailed analysis on the information brought in by TES profile retrievals into the 4D-Var assimilation system at different pressure levels is provided in Singh et al. (2010b).

Figure 3 provides the global tropospheric ozone distribution as estimated by GEOS-Chem free model run and different assimilation systems at the end of the 5 days run. The ozone concentration values are averaged over 10 GEOS-Chem levels (from the surface to about 370 hPa) for each longitude-latitude grid point on the horizontal domain.

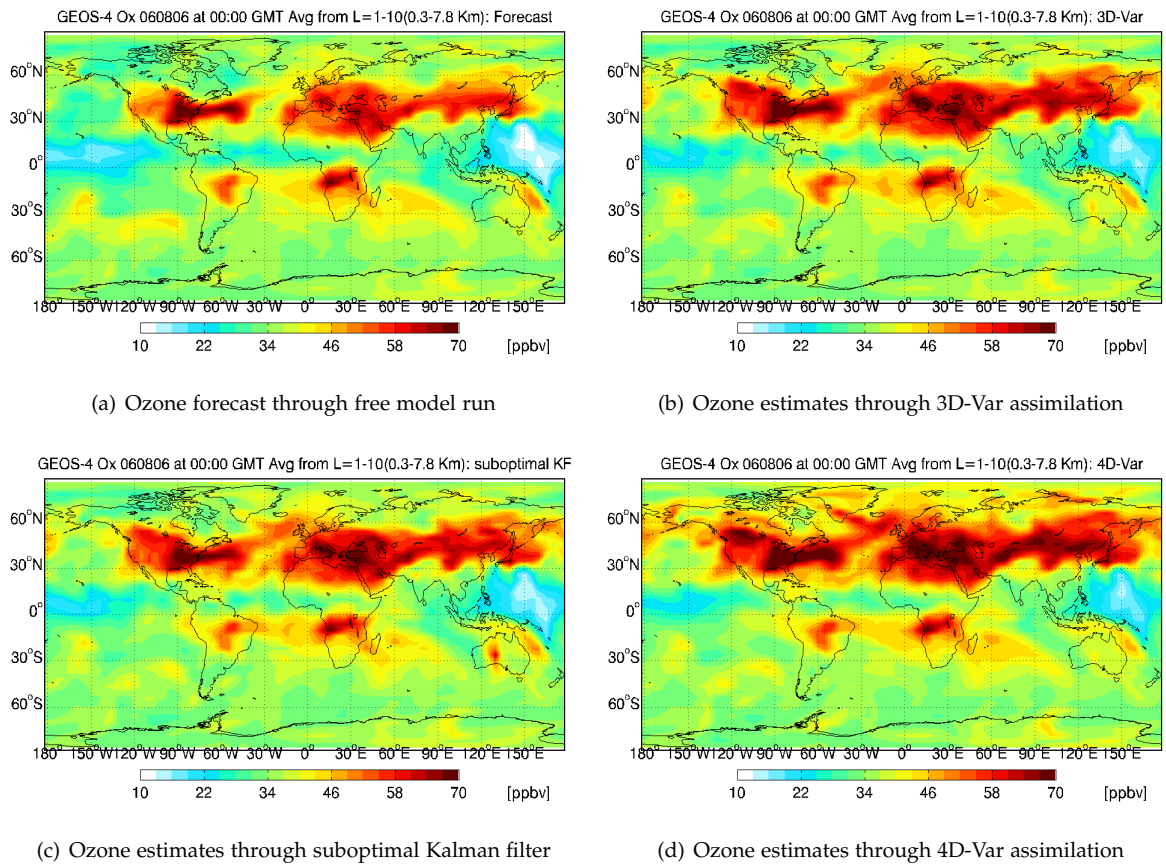


Fig. 3. Global ozone distribution at 00:00 GMT on August 6, 2006 averaged over the first 10 GEOS-Chem vertical levels. Panels (a)-(d): Global tropospheric ozone estimates provided by free model run and suboptimal KF, 3D-Var, and 4D-Var data assimilation systems from a 5-day simulation.

335 As seen in Figure 3, all the assimilation systems seem to have caused an increase in the tropospheric
 ozone as compared to the model forecast with 4D-Var bringing the highest amount. The gain seems to be
 prominent in the 30° N to 60° N latitude region in case of suboptimal KF and 3D-Var, while it is extended
 up to 90° N in case of 4D-Var. For a clear demonstration of these changes, we provide in Figure 4, the
 plots of differences in the tropospheric ozone estimates through free model run and different assimilation
 340 systems.

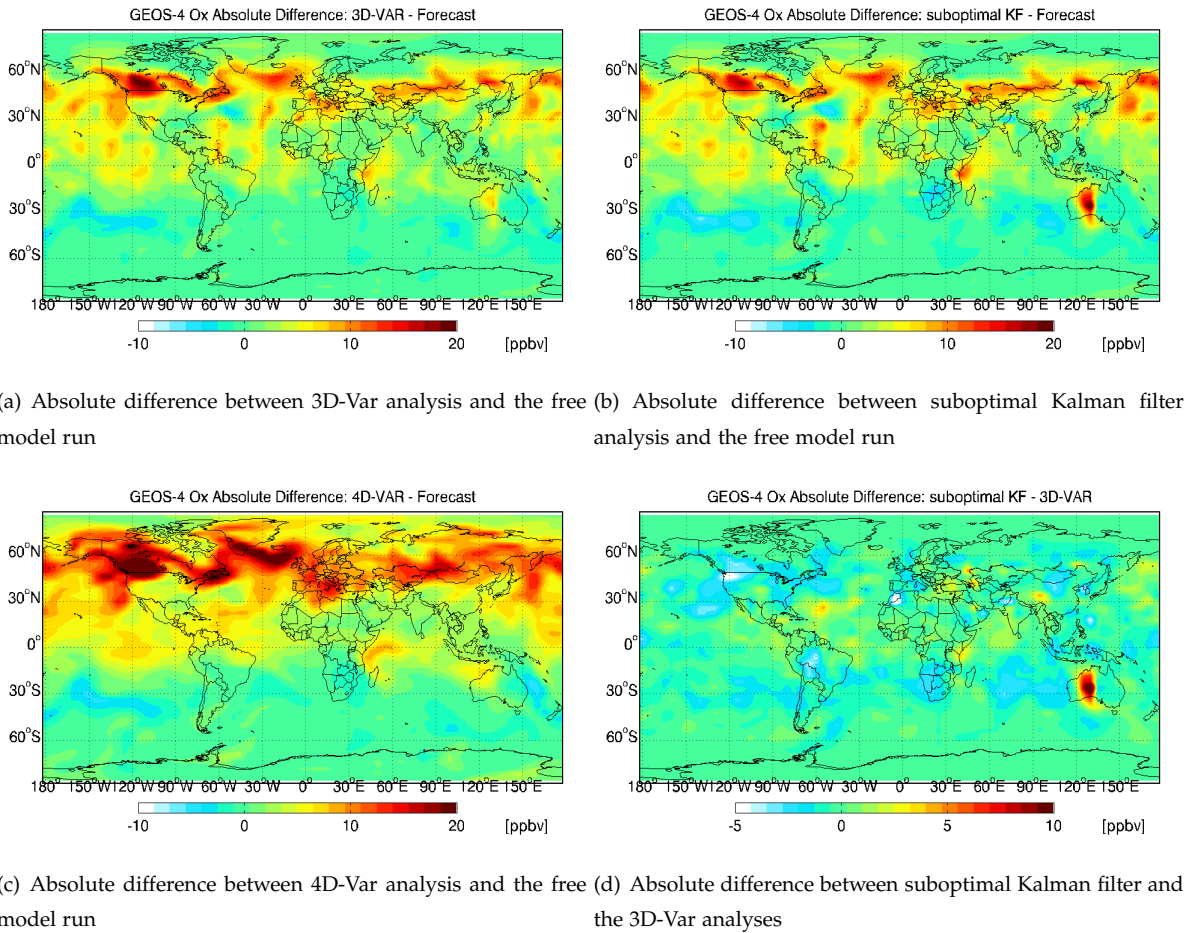


Fig. 4. Differences in global ozone concentrations at 00:00 GMT on August 6, 2006, the end of 5-day simulation, averaged over first 10 GEOS-Chem vertical levels. Panels (a)-(c): Differences between suboptimal KF, 3D-Var, and 4D-Var analysis fields and the model forecast (solution without data assimilation). Panel (d): Difference between suboptimal KF and 3D-Var analysis fields.

In Figure 4, panels (a) and (b) show that the structure of corrections in the ozone concentrations through 3D-Var and suboptimal KF data assimilation are quite similar. The reason behind such a structure is that these sequential algorithms bring in instantaneous corrections based solely on the mismatch between the model predictions and the observations in an observation window (analysis cycle). The localized correc-

345 tions here are mostly along the Aura satellite orbit. Panel (c) on the other hand showcases the smoother correction profile of 4D-Var. In each 4D-Var optimization iteration, the cost function and gradients are accumulated for all the observation windows where the adjoint variable (gradient) is flown backwards in time as governed by the model adjoint equation. The corrections brought in by the optimization routine therefore are no longer localized resulting in an ozone distribution consistent with the model dynamics and chemistry. We also plot the difference in the analysis fields obtained by 3D-Var and suboptimal KF 350 showcasing their close resemblance (panel (d)). Interestingly, there seems to be a localized overcorrection in the mid west Australian region by the suboptimal Kalman filter. This overcorrection is likely due to the propagation of emissivity errors over the Australian desert in the TES retrieval, which can have possess strong silicate spectral signatures into the TES ozone retrieval. In this case, the 4D-Var solution can smooth 355 out localized satellite artifacts through the strong model constraint.

We next consider simulations with assimilation window length of 2 weeks. A longer assimilation window provides an insight into how ozone estimates due to assimilation evolve with time and if the corrections maintain structures similar to 5-day case. In particular, the ozone lifetime will limit the utility of ozone initial condition adjustment as the assimilation window increases. It also helps adjudge if model errors 360 in GEOS-Chem cause any degradation in the assimilation systems, especially the strongly constrained 4D-Var. Similar to Figure 2, we present in Figure 5, a comparison of analysis profiles obtained from different assimilation systems against ozonesonde measurement data. The plots reflect that the accuracy of suboptimal Kalman filter and 3D-Var assimilations start to differ with longer assimilation window. While suboptimal KF underestimates ozone concentrations in the lower and mid troposphere, it performs better 365 than 3D-Var in the mid and upper tropospheric region. 4D-Var still provided the best ozone estimate of all the assimilation systems, and, unlike the 5 days assimilation window length case, it performed well in the upper tropospheric region as well except near the tropopause. Panel (c) suggests that the standard deviation of 4D-Var analysis from the ozonesonde measurements stayed the least among all the assimilation systems. The relative difference between the mean ozone analysis field and the ozonesonde 370 measurements were decreased to less than 4% up to 150 hPa as compared to 4-16% in cases of suboptimal KF and 3D-Var. With longer assimilation window, all the assimilation systems seem to have benefited from more observations being assimilated.

Figure 6 provides the global tropospheric ozone distribution as estimated by GEOS-Chem free model run and different assimilation systems. Similar to the 5 days assimilation window case, 4D-Var leads to the 375 maximum increase in the tropospheric ozone.

Figure 7 showcases the structure of corrections in model predicted ozone through different assimilation systems. The ozone corrections are up to 20 ppbv, and are consistent among the three assimilation schemes. The localized correction structure in 3D-Var and suboptimal KF cases still persists with longer assimilation window. 4D-Var provides larger corrections with a significant increase in ozone concentra-

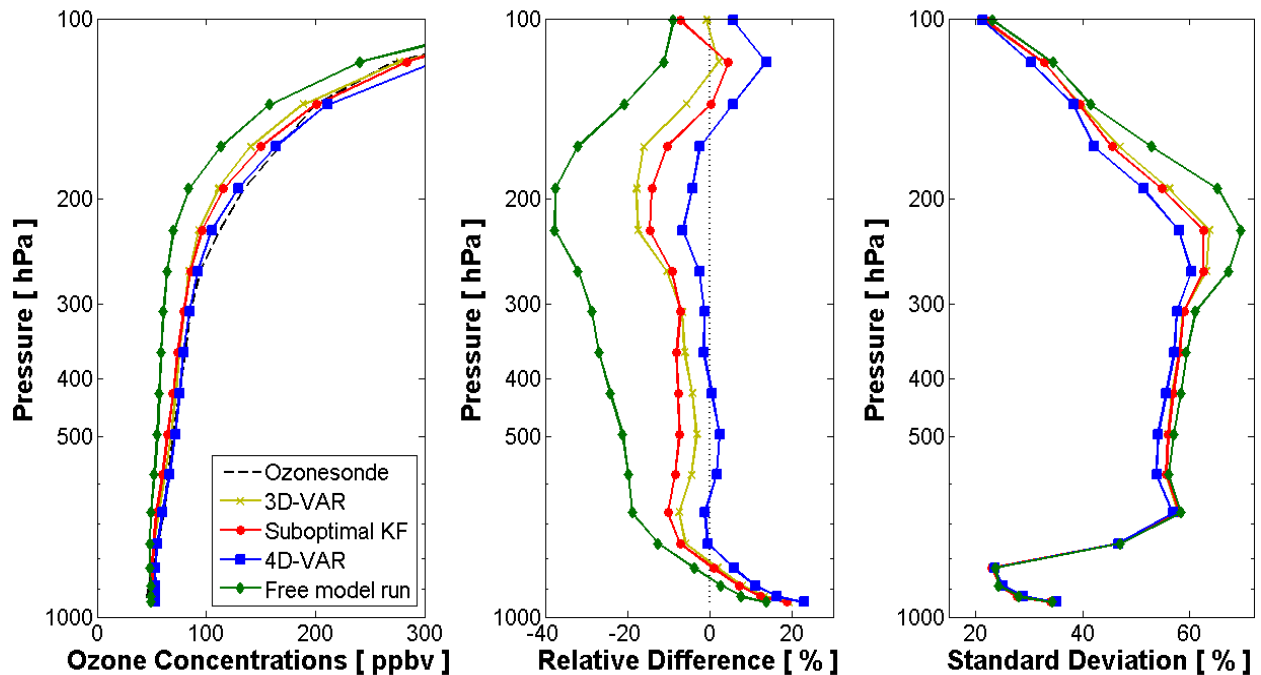


Fig. 5. The impact of ozone profile retrievals from TES on data assimilation systems for GEOS-Chem. Left panel: mean ozone concentrations at ozonesonde locations for 3D-Var, 4D-Var, suboptimal KF analyses and free model trajectories. Center panel: relative mean errors of predicted ozone concentrations with respect to ozonesonde measurements. Right panel: standard deviation of absolute values of errors with respect to ozonesonde measurements. The data is averaged over all ozonesonde launches. These plots were generated from 2 weeks simulation from 00:00 GMT August 1, 2006 to 00:00 GMT August 15, 2006 and compared against ozonesonde data available for the month of August.

380 tions in the 30° N to 90° N latitude region. The reason for this difference can be explained in part by the restriction of the TES to 60° S- 60° N, which limits where the corrections can be made in the 3D-Var. Changes poleward of 60° N in the 3D-Var solution are due to forward advection. However, as discussed in Section 6.3.2, the elevated ozone poleward of 60° N in the 4D-Var solution is due to the positive correction of high latitude initial conditions at the beginning of the assimilation window at August 1, 2006. Interest-
 385 ingly, the localized correction in the mid west Australian region which was not visible in the 3D-Var case for 5 days assimilation window case, seems to be prominent in longer assimilation, while, in the case of suboptimal KF, it has been accentuated.

Contrary to what was observed in Wu et al. (2008) for the 4D-Var assimilation in Polair3D case where the accuracy of the ozone estimates decreased with increase in the assimilation window length, our findings
 390 show that the performance of the 4D-Var system improves with increase of the assimilation window. However, this is likely due to the fact that the ozone lifetime is reasonably close to two weeks. Assimilation windows longer than two weeks would lead to a reduction in performance of the 4D-Var system as the initial conditions become less important towards the end of the window. Consequently, the assimilation

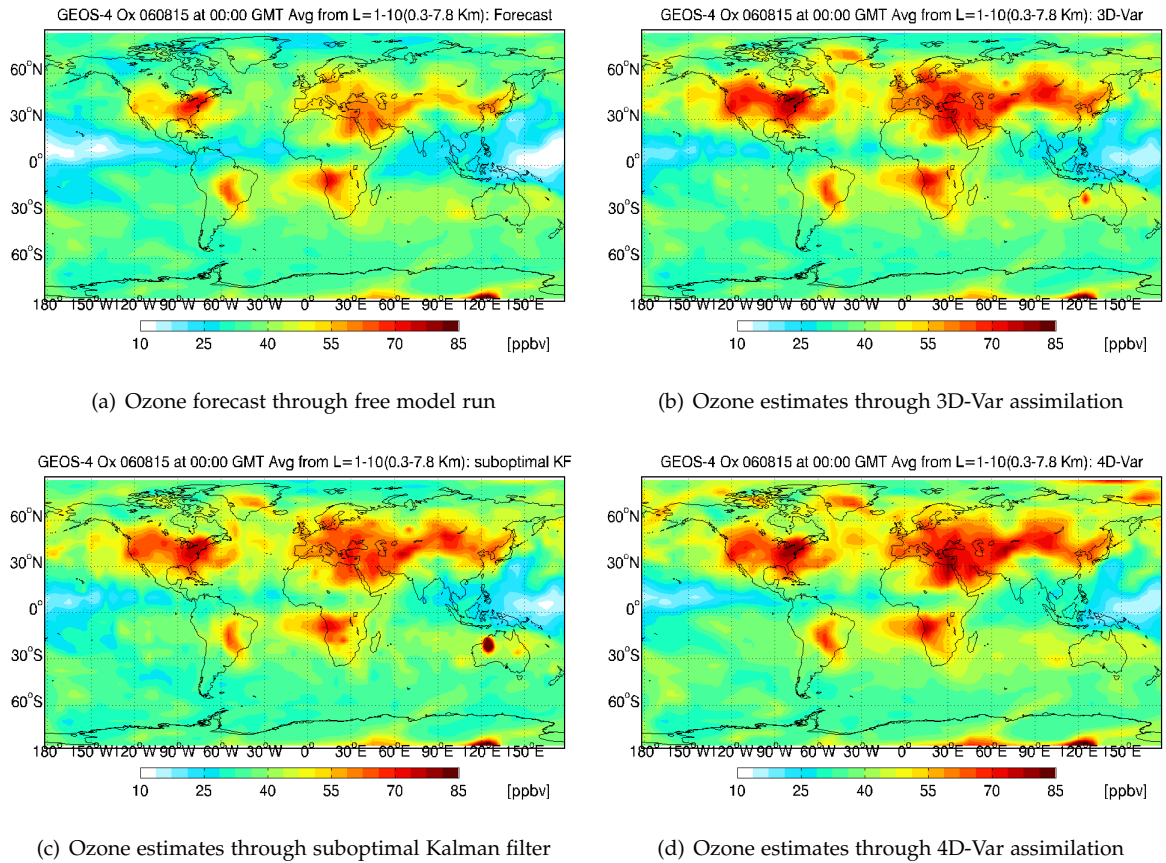
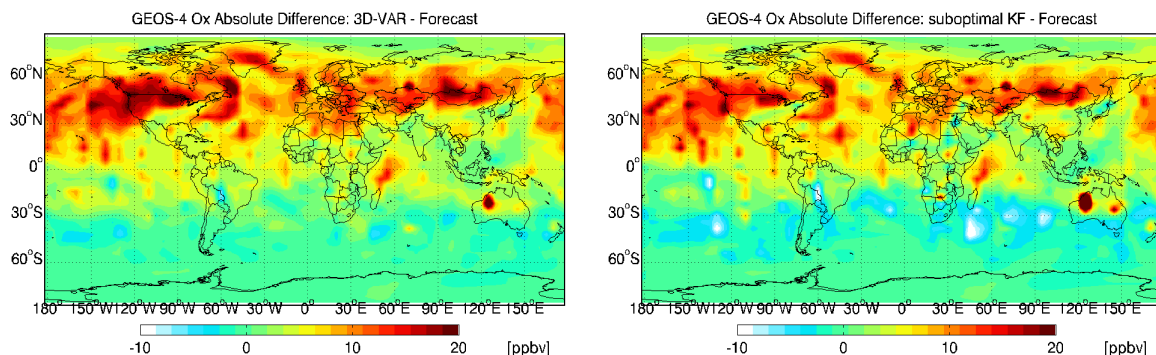


Fig. 6. Global ozone distribution at 00:00 GMT on August 15, 2006 averaged over the first 10 GEOS-Chem vertical levels. Panels (a)-(d): Global tropospheric ozone estimates provided by free model run and suboptimal KF, 3D-Var, and 4D-Var data assimilation systems from a 2-week simulation.

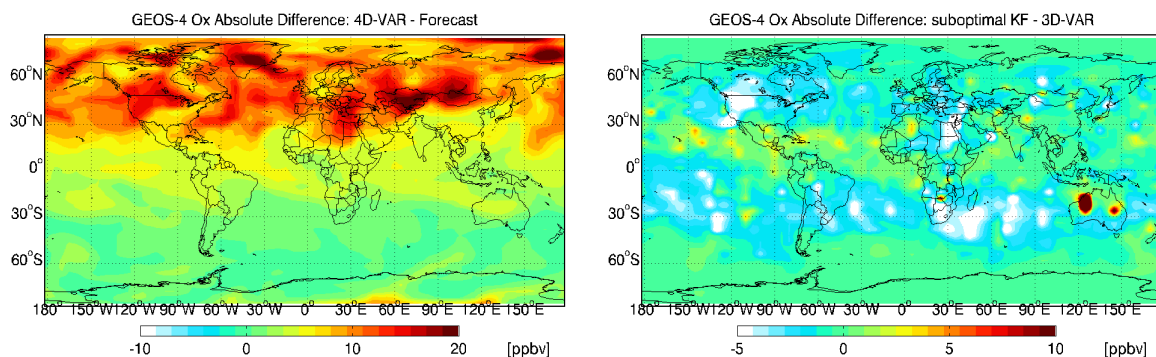
395 window for ozone in a 4D-Var system should be bounded by the ozone lifetime. There is however one case where the accuracy of ozone estimates decrease with increase in assimilation window length for 4D-Var and that is when the model adjoints are inaccurate. We have studied this case in detail in Singh et al. (2010c) and have utilized inaccurate gradients to work towards our benefit in terms of reducing significantly the memory and computational costs, still maintaining the quality of the analysis.

6.3 Comparison of 3D-Var and 4D-Var

400 As discussed in Section 2, the 3D-Var approach processes observations sequentially, and generates a new analysis every time new observations are available. The 3D-Var corrections perform successive adjustments of the forward model trajectory, which decrease the error as more observations are being considered. The 4D-Var approach, on the other hand, processes all observations at once and adjusts the initial



(a) Absolute difference between 3D-Var analysis and the free model run (b) Absolute difference between suboptimal Kalman filter analysis and the free model run



(c) Absolute difference between 4D-Var analysis and the free model run (d) Absolute difference between suboptimal Kalman filter and the 3D-Var analyses

Fig. 7. Differences in global ozone concentrations at 00:00 GMT on August 15, 2006, the end of 2-week simulation, averaged over first 10 GEOS-Chem vertical levels. Panels (a)-(c): Differences between suboptimal KF, 3D-Var, and 4D-Var analysis fields and the model forecast (solution without data assimilation). Panel (d): Difference between suboptimal KF and 3D-Var analysis fields.

conditions for the current assimilation window.

405 We compare the 3D-Var and 4D-Var approaches in two different ways. Section 6.3.1 discusses the ability of 4D-Var to explicitly represent relationships between different chemical components. Section 6.3.2 proposes a variational approach to directly compare the use of information by the two methods.

6.3.1 Dependencies between multiple species

The data assimilation scenario discussed here corrects the ozone distribution in response to new information provided by ozone measurements. The new information is distributed implicitly to other state

variables (e.g., other chemical species) through the model evolution (a change in ozone concentrations will result in different concentrations of other species after some time).

Can one explicitly represent, and apply, the corrections to other species resulting from ozone measurements? In order to perform explicit corrections of other chemical species, 3D-Var requires an inter-species error correlation matrix. A correct specification of the inter-species correlation matrix at each observation
415 time is a difficult task.

The 4D-Var approach captures the causal relationship between species through the model dynamics (this holds even when the background covariance matrix does not specify inter-chemical correlations). In principle, it is possible to directly extend the set of control variables to include the initial conditions
420 of all chemical species present in the model, together with the emission and deposition rates, and any other model parameters. The additional computational cost is minimal since the adjoint model already computes the derivatives with respect to all state variables (all concentrations), and any other sensitivity can be obtained by post-processing the adjoint fields. (Of course, extending the control vector may lead to separate issues related to convergence, and to the proper regularization of the problem).

425 The adjoint sensitivity analysis is by itself an important tool to investigate various dependencies between model parameters. The gradient formula (11) can be immediately extended to include derivatives of the cost function with respect to the initial conditions of other species besides ozone, and with respect to model parameters such as emissions and boundary conditions. The derivatives with respect to model parameters are obtained by processing the adjoint variables (Sandu et al., 2005a). The units of adjoint
430 sensitivities with respect to a parameter are one over the units of that parameter (since the cost function (9) is unitless).

Figure 8 presents the adjoint sensitivities of the 4D-Var cost function (9) with respect to several model parameters. The linearization is performed around the 4D-Var solution (10), i.e., around a forward trajectory that starts with optimized initial ozone concentrations. Consequently, the sensitivity of the 4D-Var
435 cost function with respect to the initial ozone concentration is very small (in theory is equal to zero, as it represents the gradient value at a minimum point). However, the sensitivities with respect to the initial CO (Figure 8(a)), NO_x (Figure 8(b)), and PAN (Figure 8(c)) concentrations are not small. Consequently, TES ozone profiles provide information that can potentially constrain ozone precursor initial conditions as well. More importantly, Figure 8(d) displays the sensitivity of the 4D-Var cost function with respect to
440 total NO_x emissions. These sensitivities indicate that ozone observations can be used to constrain ozone precursor emissions as well. This point is explored in the context of a 4D-Var chemical box model in Hamer et al. (2011). The strong sensitivity of the atmospheric chemical state to boundary conditions differentiates the chemical data assimilation problem from the traditional numerical weather prediction problem. Consequently, even in condition where the 3D-Var solution may have similar performance to the
445 4D-Var solution, the ability to assess the sensitivities of the innovations in the 3D-Var to boundary and

initial conditions through adjoint calculations provides important tools for a more detailed investigation of processes controlling that distribution.

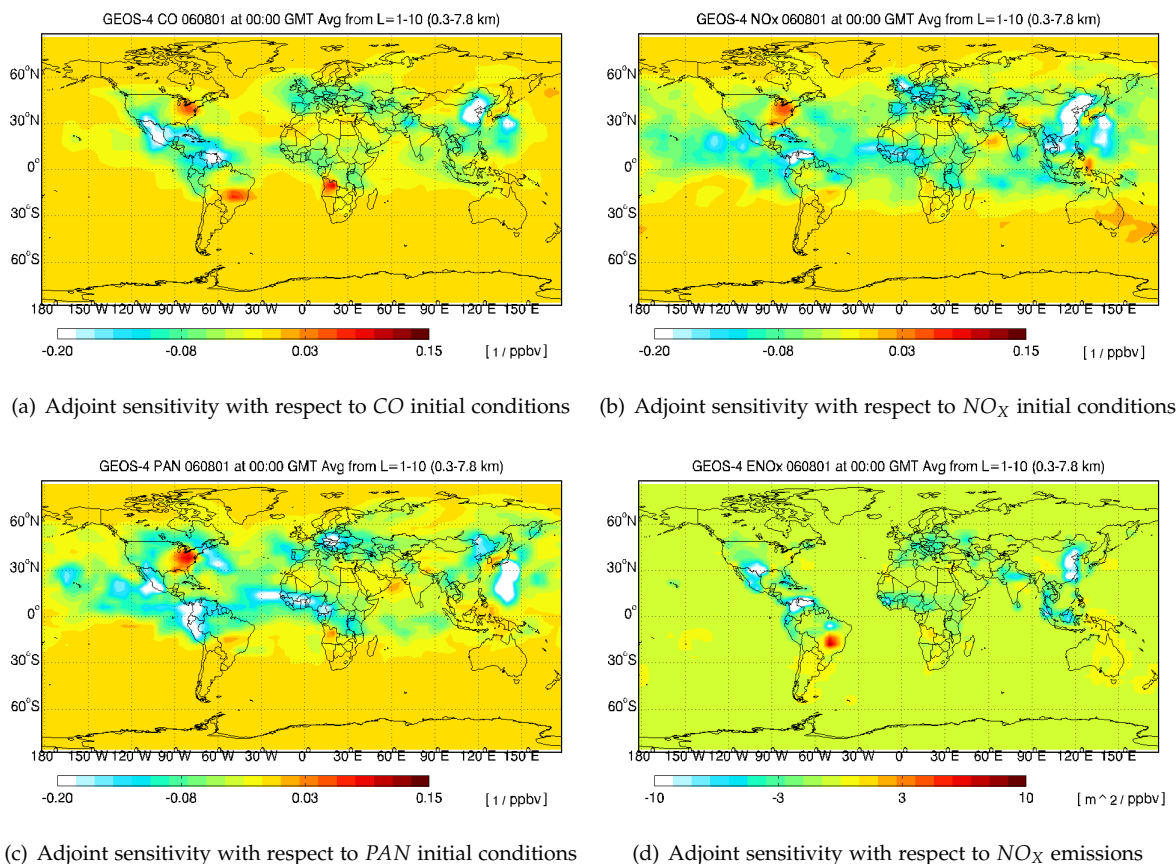


Fig. 8. Adjoint sensitivities of the 4D-Var cost function (9) with respect to different model parameters. The calculations correspond to the optimal initial ozone concentration. The 4D-Var cost function involves differences between simulated and observed O_X . Panels (a),(b),(c) show sensitivities with respect to initial conditions of other chemical species (at 00:00 GMT on August 1, 2006). The sensitivities with respect to NO_x emissions in panel (d) correspond to emissions over the entire two-week assimilation window. All sensitivity fields are averaged over the first 10 GEOS-Chem vertical levels.

6.3.2 Direct comparison of 3D-Var and 4D-Var corrections

Due to the different times when they incorporate observations, it is difficult to perform a direct comparison
 450 comparison of the ways 3D-Var and 4D-Var use this information. An assessment of the two analyses can be done at the end of the assimilation interval. The comparison against ozonesonde data, presented in Figures 2 and 5, uses analysis data at different times throughout the assimilation window.

We propose a variational approach to compare the net effect of all corrections performed by the 3D-Var,

with the 4D-Var correction of the state. This comparison provides insight into how each method injects
 455 information from observations into the state (at a specific time). We discuss three approaches, based on
 “pulling back” to the initial time and adding all corrections performed by 3D-Var, pulling back and adding
 all the differences between the 3D-Var and the 4D-Var analyses, and finding an equivalent initial condition
 for 3D-Var.

To be specific, we first quantify the cumulative effect of all 3D-Var corrections, in order to study how
 3D-Var builds the analysis. Since the 3D-Var corrections take place at different times, they need to first be
 brought to the same time. For example, this can be done by “propagating backwards” the 3D-Var
 correction at t_i to the initial time t_0 , through the adjoint \mathbf{M}_i^T of the tangent linear model $\mathbf{M}_i = \partial \mathbf{x}_i / \partial \mathbf{x}_0$. The
 cumulative effect of all 3D-Var corrections at the initial time is

$$\sum_{i=0}^N \mathbf{M}_k^T \cdot \mathbf{P}_i^{f(3)} \mathbf{H}_i^T \left(\mathbf{H}_i \mathbf{P}_i^{f(3)} \mathbf{H}_i^T + \mathbf{R}_i \right)^{-1} \left(\mathbf{y}_i - \mathcal{H}(\mathbf{x}_i^{f(3)}) \right). \quad (22)$$

Here $\mathbf{x}_i^{f(3)}$ and $\mathbf{P}_i^{f(3)}$ are the 3D-Var forecast state and the forecast covariance at t_i , respectively. This
 460 approach allows for the assessment of the cumulative effect of all 3D-Var corrections at the initial time,
 and to directly compare the 3D-Var and 4D-Var via the corresponding changes in initial conditions.

Next, we seek to estimate the discrepancy between the analyses generated by the 3D-Var and by the 4D-
 Var methods. Let the free model run (background), the 4D-Var, and the 3D-Var analyses at t_i be \mathbf{x}_i^b , $\mathbf{x}_i^{a(4)}$,
 $\mathbf{x}_i^{a(3)}$, respectively. Define the following “discrepancy” cost function that measures the difference between
 the 4D-Var and the 3D-Var analyses at all times

$$\mathcal{D} \left(\mathbf{x}_0^{a(4)} \right) = \frac{1}{2} \sum_{i=0}^N \left\| \mathbf{x}_i^{a(4)} - \mathbf{x}_i^{a(3)} \right\|_{\mathbf{Q}_i^{-1}}^2. \quad (23)$$

The gradient of the discrepancy function with respect to the initial conditions is given by the adjoint
 model, using a linearization of the forward model about the 4D-Var analysis trajectory

$$\nabla_{\mathbf{x}_0^a} \mathcal{D} \left(\mathbf{x}_0^{a(4)} \right) = \sum_{i=0}^N \mathbf{M}_i^T \mathbf{Q}_i^{-1} \left(\mathbf{x}_i^{a(4)} - \mathbf{x}_i^{a(3)} \right), \quad \text{where } \mathbf{M}_i = \frac{\partial \mathbf{x}_i^{a(4)}}{\partial \mathbf{x}_0^{a(4)}}. \quad (24)$$

Here \mathbf{M}_i is the linearized model solution operator about the 4D-Var analysis trajectory. Each term in the
 discrepancy sum is weighed by the (covariance-like) matrix \mathbf{Q}_i , which is assumed to be invertible. This
 adjoint considers the differences between the 4D-Var and the 3D-Var analyses at different times, and pulls
 all these differences back to time t_0 . The cumulative discrepancy between the two analyses, as given by
 this metric, reads

$$\text{diff} \left(\mathbf{x}^{a(4)}, \mathbf{x}^{a(3)} \right) = \nabla_{\mathbf{x}_0^a} \mathcal{D} \left(\mathbf{x}_0^{a(4)} \right). \quad (25)$$

Finally, we want to determine the “3D-Var equivalent initial condition” $\mathbf{x}_0^{e(3)}$, such that the resulting tra-
 jectory $\mathbf{x}_i^{e(3)}$, $i \geq 1$, fits best the 3D-Var analysis at the final time $\mathbf{x}_N^{a(3)}$, in a least squares sense:

$$\mathbf{x}_0^{e(3)} = \underset{\mathbf{x}_0}{\text{argmin}} \mathcal{B} \left(\mathbf{x}_0^{e(3)} \right) = \frac{1}{2} \left\| \mathbf{x}_N^{e(3)} - \mathbf{x}_N^{a(3)} \right\|_{\mathbf{Q}_N^{-1}}^2.$$

To our knowledge, no attempt has been made to date to estimate the equivalent effect of all 3D-Var corrections at the initial time. (Note that the 3D-Var analysis is not a trajectory of the model). The methodology is explained in Appendix A. The least squares solution to finding the 3D-Var equivalent initial condition is (A3)

$$\mathbf{x}_0^{e(3)} = \mathbf{x}_0^{a(4)} - \left(\mathbf{M}_N^T \mathbf{Q}_N^{-1} \mathbf{M}_N \right)^{-1} \cdot \mathbf{M}_N^T \mathbf{Q}_N^{-1} \left(\mathbf{x}_N^{e(3)} - \mathbf{x}_N^{a(3)} \right),$$

The 3D-Var solution incorporates all the observation information when it reaches t_N , the end of the assimilation window. For a direct comparison with the 4D-Var initial condition, the 3D-Var equivalent initial condition match the 3D-Var analysis only at the final time.

465 Similar to (23), a cost function that measures the discrepancy between the 3D-Var and the free model forecast at all times can be defined. This gradient involves an adjoint run, with a linearization performed about the free model run (background) trajectory.

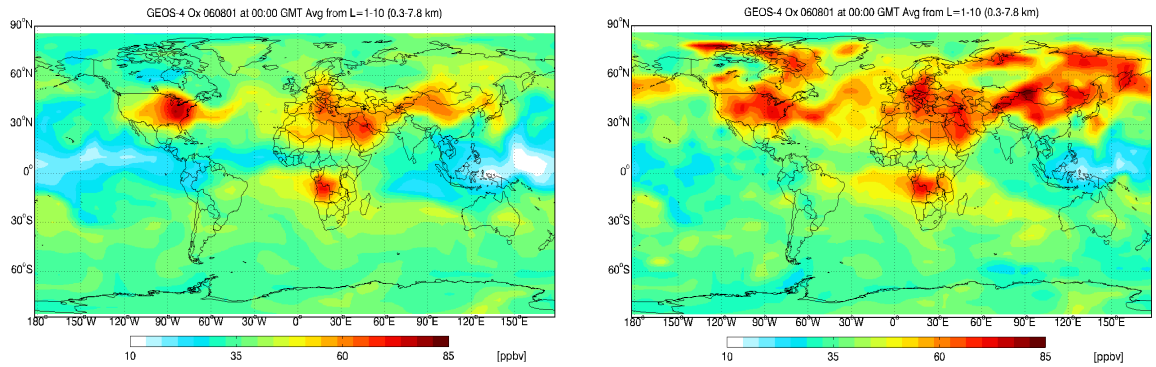
Figure 9 displays results for the metric (25), i.e., the sum of all analysis discrepancies between the 3D-Var and the 4D-Var ozone analyses, projected to time t_0 along with differences between the free running model
470 and the initial conditions inferred from the 4D-Variational solution. All scaling covariances are taken to be the identity matrix, $\mathbf{Q}_i = \mathbf{I}$, $i = 0, \dots, N$. Interestingly, significant corrections to the initial conditions in the 4D-Var solution are made poleward of 60°N even though there is no TES data used that directly covers that region. These positive corrections can be explained by strong transport from higher latitudes into the mid-latitudes characterized by the transport adjoint sensitivities of the mid-latitude innovations with the
475 TES data. Similar features are seen though in the opposite sign in Figure 9(d) through the cumulative back projection in the 3D-Var solution.

7 Conclusions

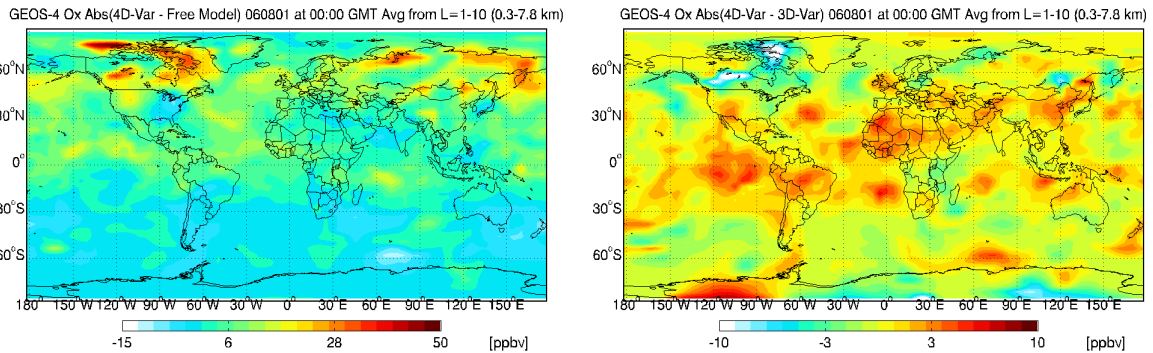
This paper compares the performance of 3D-Var, 4D-Var, and suboptimal Kalman filter data assimilation systems, applied to the estimation of global tropospheric ozone distribution. The data is provided by TES
480 ozone profile retrievals. The study uses the 3D-Var and 4D-Var data assimilation frameworks we have implemented into GEOS-Chem v7. Two different assimilation window lengths (five days and two weeks) are considered. The quality of the ozone analyses provided by different assimilation schemes is verified against ozonesonde measurements, an independent data set.

The three approaches have different computational costs. The suboptimal Kalman filter is the least expensive, followed closely by 3D-Var. 4D-Var has the highest memory and computational costs as it requires
485 checkpointing dependent variables, and performs both a forward and an adjoint model run for every iteration.

All three data assimilation systems are able to improve ozone estimates using TES profile retrievals. For



(a) Free model ozone concentration at the beginning of the assimilation window (b) 4D-Var ozone analysis at the beginning of the assimilation window



(c) Absolute difference between the 4D-Var optimal initial condition, and the background initial condition (d) Cumulative difference between the 4D-Var and 3D-Var analyses throughout the assimilation window

Fig. 9. The cumulative difference (25) between the 4D-Var and the 3D-Var ozone analyses, projected at the beginning of the five days assimilation window, and averaged over the first 10 GEOS-Chem vertical levels. A two-week long data assimilation window is used, starting at 00:00 GMT on August 1, 2006.

the five days assimilation window the sequential methods, 3D-Var and suboptimal KF, perform similarly:
 490 they decrease the relative difference between mean analysis and ozonesonde measurements to about 5-20%. 4D-Var, on the other hand, brings this error down to less than 4%, for up to 180 hPa. For the two weeks assimilation window the performance of the sequential methods changes with different height levels. In the lower and mid troposphere 3D-Var performs better, while in the mid to upper troposphere the suboptimal Kalman filter analysis is more accurate. The relative error (measured against ozonesonde
 495 data) is 4-16% for the sequential analyses, and is less than 4% for up to 150 hPa for 4D-Var. The corrections of ozone concentration performed by the sequential assimilation methods are localized along the satellite orbit. On the other hand, the 4D-Var solution is physically and chemically self-consistent over the assimilation window. The region between latitudes 30° N to 60° N has the greatest impact from all the assimilation systems. This region extends up to 90° N in case of 4D-Var, which accounts for the transport

500 of high latitude ozone into the mid-latitudes. However, we should caution that the IONS datasets were primarily over North America. Therefore, we can not assess whether the increased northern mid-latitude ozone concentrations lead to a more accurate analysis.

A method to directly compare the analyses provided different schemes is proposed, based on “pulling back” differences to the initial time, as discussed in Section 6.3.2. The calculations show that the 4D-
505 Var corrections are larger than those provided by 3D-Var. The adjoint sensitivity analysis in section 6.3.1 reveals that 4D-Var has the intrinsic capability of capturing mechanistic relationships between multiple chemical species, and between emissions and concentrations fields. In a similar vein, this adjoint analysis can be used in conjunction with other assimilation schemes (3D-Var, suboptimal KF) to interrogate what model parameters are driving the residual differences with the observations.

510 The comparison results presented here will guide the choice of the best assimilation scheme for the problem at hand. The sub-optimal Kalman filter and the 3D-Var solution provide useful solutions that do not require significant changes as the forward model physics and chemistry are updated. By virtue of their simplicity, they make less model assumptions, e.g., all differences between observation and forecast can be attributed to initial conditions, and therefore can be robust under a variety of conditions. On the other
515 hand, the 4D-Var approach provides a physically consistent solution where uncertainties are ascribed to a combination of initial and boundary conditions. This physical consistency makes it more straightforward to interpret and make scientific inferences. We have introduced a new method that applies the adjoint sensitivity to help interpret the 3D-Var solutions, which provides a kind of middle ground between the more efficient 3D-Var approach and the more sophisticated 4D-Var approaches. Interesting extensions of
520 the GEOS-Chem data assimilation framework, such as efficient information content estimation of observations and construction of full rank covariance matrices, are discussed in companion papers Singh et al. (2010a,b,c).

Acknowledgements

This work was supported by NASA through the ROSES-2005 AIST project. The work of A. Sandu was
525 also partially supported by NSF through the award NSF DMS-0915047.

The authors would like to thank Professor Anne Thompson of Pennsylvania State University and Dr. David Tarasick of Environment Canada who led the IONS-6 campaign, and who provided the IONS data used in this work.

References

- 530 Beer, R., Glavich, T. A., and Rider, D. M.: Tropospheric emission spectrometer for the Earth Observing System's Aura satellite, *Appl. Opt.*, 40(15), 2356-2367, 2001.
- Bei, N., de Foy, B., Lei, W., Zavala, M., and Molina, L. T.: Using 3DVAR data assimilation system to improve ozone simulations in the Mexico City basin, *Atmos. Chem. Phys.*, 8, 7353-7366, doi:10.5194/acp-8-7353-2008, 2008.
- Benkovitz, C. M., Scholtz, M. T., Pacyna, J., Tarrason, L., Dignon, J., Voldner, E. C., Spiro, P. A., Logan, J. A., and
535 Graedel, T. E.: Global gridded inventories of anthropogenic emissions of sulfur and nitrogen, *J. Geophys. Res.*, 101(D22), 29,239-29,253, 1996.
- Bey, I., Jacob, D. J., Yantosca, R. M., Logan, J. A., Field, B., Fiore, A. M., Li, Q., Liu, H., Mickley, L. J. and Schultz, M.: Global modeling of tropospheric chemistry with assimilated meteorology: Model description and evaluation, *J. Geophys. Res.*, 106, 23, 073-23,096, 2001.
- 540 Blum, J., Le Dimet, F. X., Navon, I. M.: Data Assimilation for Geophysical Fluids, Chapter in *Computational Methods for the Atmosphere and the Oceans*, Volume 14, Elsevier Science Ltd, New York, ISBN-13: 978-0-444-51893-4, 2009.
- Boutahar, J., Lacour, S., Mallet, V., Quélo, D., Roustan, Y., and Sportisse, B.: Development and validation of a fully modular platform for numerical modelling of air pollution: POLAIR, *International Journal of Environment and Pollution*, 22(1/2):17-28, 2004.
- 545 Bowman, K. W., Worden, J., Steck, T., Worden, H. M., Clough, S. and Rodgers, C.: Capturing time and vertical variability of tropospheric ozone: A study using TES nadir retrievals, *J. Geophys. Res.*, 107, (D23), 2007.
- Bowman, K. W., Rodgers, C. D., et al: Tropospheric Emission Spectrometer: Retrieval method and error analysis, *IEEE Transactions on Geoscience and Remote Sensing*, vol. 44, no. 5, May 2006.
- K. W. Bowman, D. B. A. Jones, J. A. Logan, H. Worden, F. Boersma, R. Chang, S. Kulawik, G. Osterman, P. Hamer, and
550 J. Worden. The zonal structure of tropical O₃ and CO as observed by the Tropospheric Emission Spectrometer in November 2004 Part 2: Impact of surface emissions on O₃ and its precursors. *Atmos. Chem. Phys.*, 9(11):3563-3582, 06 2009/06/03.
- Carmichael, G. R., Sandu, A., Chai, T., Daescu, D., Constantinescu, E. M. and Tang, Y.: Predicting air quality: Improvements through advanced methods to integrate models and measurements, *Journal of Computational Physics*,
555 Vol. 227, Issue 7, p. 3540-3571, 2008.
- Chai, T., Carmichael, G. R., Sandu, A., Tang, Y. and Daescu, D. N.: Chemical data assimilation of transport and chemical evolution over the Pacific (TRACE-P) aircraft measurements, *Journal of Geophysical Research*, 111, D02301, doi:10.1029/2005JD005883, 2006.
- Chai, T., Carmichael, G. R., Tang, Y., Sandu, A., Hardesty, M., Pilewskie, P., Whitlow, S., Browell, E. V., Avery, M. A.,
560 Thouret, V., Nedelec, P., Merrill, J. T. and Thomson, A. M.: Four dimensional data assimilation experiments with ICARTT (International Consortium for Atmospheric Transport and Transformation) ozone measurements, *Journal of Geophysical Research*, Vol. 112, D12S15, doi:10.1029/2006JD007763, 2007.
- Chai, T., Carmichael, G. R., Tang, Y. and Sandu, A.: Regional NO_x emission inversion through a four-dimensional variational approach using SCIAMACHY tropospheric NO₂ column observations, *Atmospheric Environment*,
565 doi:10.1016/j.atmosenv.2009.06.052, in print, 2009.
- Clark, H. L., Cathala, M. -L., Teysse'dre, H., Cammas, J. -P. and Peuch, V. -H.: Cross-tropopause fluxes of ozone using assimilation of MOZAIC observations in a global CTM, *Tellus, Ser. A and Ser. B*, 59B, 39-49, 2006.

- Cohn, S., Da Silva, A., Guo, J., Sienkiewicz, M., and Lamich, D.: Assessing the Effects of Data Selection with DAO's Physical-space Statistical Analysis System, *Monthly Weather Review*, 126, 2913-2926, 1998.
- 570 Constantinescu, E. M., Sandu, A., Chai, T. and Carmichael, G. R.: Investigation of ensemble-based chemical data assimilation in an idealized setting, *Atmospheric Environment*, Vol. 41, Issue 1, p. 18–36, 2007.
- Constantinescu, E. M., Sandu, A., Chai, T. and Carmichael, G. R.: Ensemble-based chemical data assimilation. I: General approach, *Quarterly Journal of the Royal Meteorological Society*, Volume 133, Issue 626, p. 1229–1243, Online ISSN: 1477-870X, Print ISSN: 0035-9009, July 2007 Part A.
- 575 Constantinescu, E. M., Sandu, A., Chai, T. and Carmichael, G. R.: Ensemble-based chemical data assimilation. II: Covariance localization, *Quarterly Journal of the Royal Meteorological Society*, Volume 133, Issue 626, p. 1245–1256, Online ISSN: 1477-870X, Print ISSN: 0035-9009, July 2007 Part A.
- Cooper, O. R., et al.: Large upper tropospheric ozone enhancements above midlatitude North America during summer: In situ evidence from the IONS and MOZAIC ozone measurement network, *J. Geophys. Res.*, 111, D24S05, doi:10.1029/2006JD007306, 2006.
- 580 Cooper, O. R., et al.: Evidence for a recurring eastern North American upper tropospheric ozone maximum during summer, *J. Geophys. Res.*, 112, D23304, doi:10.1029/2007JD008710, 2007.
- Courtier, P. and Talagrand, O.: Variational assimilation of meteorological observations with the adjoint vorticity equations II: Numerical results, *Quart. J. Roy. Meteor. Soc.* 113, 1329-1347, 1987.
- 585 Courtier, P., Andersson, E., Heckley, W., Pailleux, J., Vasiljevic, D., Hamrud, M., Hollingsworth, A., Rabier, F. and Fisher, M.: The ECMWF implementation of three-dimensional variational assimilation (3D-Var) I: Formulation, *Quarterly Journal of the Royal Meteorological Society*, 124(550):1783, 1998.
- Daescu, D., Carmichael, G.R., and Sandu, A.: Adjoint Implementation of Rosenbrock Methods Applied to Variational Data Assimilation Problems, *J. Comp. Phys.* 165, 496-510, 2000.
- 590 Daescu, D., Sandu, A., and Carmichael, G.R.: Direct and Adjoint Sensitivity Analysis of Chemical Kinetic Systems with KPP: II - Validation and Numerical Experiments, *Atmos. Environ.*, 37, 5097-5114, 2003.
- Daescu, D.N.: On the sensitivity equations of four-dimensional variational (4D-Var) data assimilation, *Monthly Weather Review*, 136 (8), 3050-3065, 2008.
- Daley, R.: *Atmospheric Data Analysis*, Cambridge University Press, p. 457pp, 1991.
- 595 Damian, V., Sandu, A., Damian, M., Potra, F., and Carmichael, G.R.: The Kinetic PreProcessor KPP - A Software Environment for Solving Chemical Kinetics, *Comp. and Chem. Eng.*, 26, 11, 1567-1579, 2002.
- Derber, J. C., Parrish, D. F., Lord, S. J.: The New Global Operational Analysis System at the National Meteorological Center. *Weather and Forecasting*, 6, 538-547, 1991.
- Duncan, B. N., Martin, R. V., Staudt, A. C., Yevich, R., and Logan, J. A.: Interannual and seasonal variability of biomass burning emissions constrained by satellite observations, *J. Geophys. Res.*, 108(D2), 4100, doi:10.1029/2002JD002378, 2003.
- 600 Elbern, H. and H. Schmidt: Ozone episode analysis by four dimensional variational chemistry data assimilation, *J. Geophys. Res.*, 106(D4), 3569–3590, 2001.
- Eller, P., Singh, K., Sandu, A., Bowman, K. W., Henze, D. K. and Lee, M.: Implementation and evaluation of an array of chemical solvers in a global chemical transport model, *Geophysical Model Development*, Vol. 2, p. 1–7, 2009.
- 605 Evensen, G.: Sequential data assimilation with a nonlinear quasi-geostrophic model using Monte Carlo methods to forecast error statistics, *J. Geophys. Res.* 99, 10143–10162, 1994.

- Geer, A. J., et al.:The ASSET intercomparison of ozone analyses: Method and first results, *Atmos. Chem. Phys.*, 6, 5445–5474, 2006.
- 610 Gaspari, G., Cohn, S. E.: Construction of correlation functions in two and three dimensions, *Quarterly Journal of the Royal Meteorological Society*, Vol 125 Issue 554,723-757, 1999.
- Gauthier, P., Charette, C., Fillion, L., Koclas, P. and Laroche, S.: Implementation of a 3D Variational Data Assimilation System at the Canadian Meteorological Centre. Part I: The Global Analysis, *Atmosphere-Ocean*, 37 (2), 103–156, 1999.
- 615 Hakami, A., Henze, D. K., Seinfeld, J. H., Chai, T., Tang, Y., Carmichael, G.R. and Sandu, A.: Adjoint inverse modeling of black carbon during ACE-Asia, *Journal of Geophysical Research*, Vol. 110, D14301, doi:10.1029/2004JD005671, 25 pages, 2005.
- Hakami A., Henze D.K., Seinfeld J.H., et al.: The adjoint of CMAQ. *Environmental Science and Technology*, 41(22):7807–7817, 2007.
- 620 Hamer, P., Bowman, K., Henze D., :Observing requirements for geostationary satellites to enable ozone air quality prediction, *Atmos. Chem. Phys.*, *submitted*
- Henze D.K., Seinfeld J.H., Liao W., Sandu A., et al.: Inverse modeling of aerosol dynamics: Condensational growth . *Journal of Geophysical Research-Atmospheres*, Volume: 109, Issue: D14, Article Number: D14201, 2004.
- Henze, D. K., Hakami, A. and Seinfeld, J. H.: Development of the adjoint of GEOS-Chem, *Atmos. Chem. Phys.*, 7, 2413-2433, 2007.
- 625 Henze, D. K., Seinfeld, J. H. and Shindell, D. T.: Inverse modeling and mapping U.S. air quality influences of inorganic PM_{2.5} precursor emissions with the adjoint of GEOS-Chem, *Atmos. Chem. Phys.*, 9, 5877-5903, 2009.
- Horowitz, L. W., et al.: A global simulation of tropospheric ozone and related tracers: Description and evaluation of MOZART, version 2, *J. Geophys. Res.*, 108(D24), 4784, doi:10.1029/2002JD002853, 2003.
- 630 Horowitz, L. W.: Past, present and future concentrations of tropospheric ozone and aerosols: Methodology, ozone evaluation, and sensitivity to aerosol wet removal, *J. Geophys. Res.*, 111, D22211, doi:10.1029/2005JD006937, 2006.
- Houtekamer, P. L., Mitchell, H. L., Pellerin, G., Buehner, M., Charron, M., Spacek, L., and Hansen, B.: Atmospheric Data Assimilation with an Ensemble Kalman Filter: Results with Real Observations, *Monthly Weather Review*, 133(3):604-620, 2005.
- 635 Hudman, R. C., et al.: Surface and lightning sources of nitrogen oxides over the United States: Magnitudes, chemical evolution and outflow, *J. Geophys. Res.*, 112, D12S05, doi:10.1029/2006JD007912, 2007.
- D. J. Jacob. *Introduction to Atmospheric Chemistry*. Princeton University Press, New Jersey, 1999.
- Jones, D. B. A., Bowman, K. W., Logan, J. A., Heald, C. L., Liu, J., Luo, M., Worden, J. and Drummond, J.: Inversion analysis of carbon monoxide emissions using data from the TES and MOPITT satellite instruments, *Atmospheric Chemistry and Physics Discussions*, 7, 17625–17662, 2007.
- 640 Jones, D. B. A., Bowman, K. W., Palmer, P. I., Worden, J. R., Jacob, D. J., Hoffman, R. N., Bey, I. and Yantosca, R. M.: Potential of observations from the Tropospheric Emission Spectrometer to constrain continental sources of carbon monoxide, *J. Geophys. Res.*, 108, (D24), 2003.
- Kalnay, E.: *Atmospheric modeling, data assimilation and predictability*, Cambridge University Press, 2002.
- 645 Khattatov, B. V., Gille, J. C., Lyjak, L. V., Brasseur, G. P., Dvortsov, V. L., Roche, A. E. and Walters, J.: Assimilation of photochemically active species and a case analysis of UARS data, *Journal of Geophysical Research*, 104:18715–18737, 1999.

- Khattatov, B. V., Lamarque, J. -F., Lyjak, L. V., Menard, R., Levelt, P., Tie, X., Brasseur, G. P. and Gille, J. C.: Assimilation of satellite observations of long-lived chemical species in global chemistry transport models, *J. Geophys. Res.*, 650 105(D23), 29–135, 2000.
- Kopacz, M., Jacob, D. J., Henze, D. K., Heald, C. L., Streets, D. G., and Zhang, Q.: A comparison of analytical and adjoint Bayesian inversion methods for constraining Asian sources of CO using satellite (MOPITT) measurements of CO columns, *Journal of Geophysical Research*, 2007, 114, D04305.
- Lahoz, W. A., et al.: The Assimilation of Envisat data (ASSET) project, *Atmos. Chem. Phys.*, 7, 1773-1796, 2007.
- 655 Lamarque, J.-F., Khattatov, B. V. and Gille, J. C.: Constraining tropospheric ozone column through data assimilation, *J. Geophys. Res.*, 107(D22), 4651, doi:10.1029/2001JD001249, 2002.
- Laroche, S., Dorval, E. C., Canada, Q. C., Gauthier, P., Tanguay, M., Pellerin, S., and Morneau, J.: Evaluation of the operational 4D-Var at the Meteorological Service of Canada, 21st Conference on Weather Analysis and Forecasting, 14B.3, 2005.
- 660 LeDimet, F.-X. and Talagrand, O.: Variational algorithms for analysis and assimilation of meteorological observations: theoretical aspects, *Tellus* 38A, 97-110, 1986.
- Li, Z. and Navon, I. M.: Optimality of variational data assimilation and its relationship with the Kalman filter and smoother, *Q. J. R. Meteorol. Soc.*, 127, pp. 661-683, 2001.
- Li, Q., Jacob, D. J., Park, R. J., Wang, Y., Heald, C. L., Hudman, R. C., Yantosca, R. M., Martin, R. V., and Evans, M. 665 J.: North American pollution outflow and the trapping of convectively lifted pollution by upper-level anticyclone, *J. Geophys. Res.*, 110, D10301, doi:10.1029/2004JD005039, 2005.
- Liao WY, Sandu A, Carmichael GR, et al.: Singular vector analysis for atmospheric chemical transport models, *Monthly Weather Review*, 134(9):2443–2465, 2006.
- Lions, J. L.: *Optimal control of systems governed by partial differential equations*, Springer-Verlag, 1971.
- 670 Logan, J. A.: Trends in the vertical distribution of ozone: An analysis of ozonesonde data, *J. Geophys. Res.*, 99(D12), 25,553-0–25,585, 1994.
- Logan, J. A.: An analysis of ozonesonde data for the troposphere: Recommendations for testing 3-D models and development of a gridded climatology for tropospheric ozone, *J. Geophys. Res.*, 104(D13), 16,115–16,149, 1999.
- McLinden, C. A., Olsen, S. C., Hannegan, B., Wild, O., Prather, M. J., and Sundet, J.: Stratospheric ozone in 675 3-D models: A simple chemistry and the cross-tropopause flux, *J. Geophys. Res.*, 105(D11), 14,653–14,665, doi:10.1029/2000JD900124, 2000.
- Menard, R., Cohn, S. E., Chang, L. -P. and Lyster, P. M.: Assimilation of stratospheric chemical tracer observations using a Kalman Filter I: Formulation, *Mon. Weather Rev.*, 128, 2654-2671, 2000.
- Munro, R., Siddans, R., Reburn, W. J., and Kerridge, B. J.: Direct measurement of tropospheric ozone distributions 680 from space, *Nature*, 392(6672), 168–171, 1998.
- Nassar, R., Logan, J. A., Worden, H. M., et al.: Validation of Tropospheric Emission Spectrometer (TES) nadir ozone profiles using ozonesonde measurements, *J. Geophys. Res.*, 113, D15S17, doi:10.1029/2007JD008819, 2008.
- Navon, I. M.: Data assimilation for Numerical Weather Prediction: a review, in: *Data Assimilation for Atmospheric, Oceanic, and Hydrologic Applications*, XVIII, 475 p. 326 illus., Hardcover, ISBN: 978-3-540-71055-4, 2009.
- 685 Oltmans, S. J., et al.: Long-term changes in tropospheric ozone, *Atmos. Environ.*, 40, 3156–3173, 2006.
- Ott, E., Hunt, B. R., Szunyogh, I., Zimin, A.V., Kostelich, E. J., Kostelich, M., Corazza, M., Sauer, T., Kalnay, E., Patil, D. J. and Yorke, J. A.: A local ensemble Kalman Filter for Atmospheric Data Assimilation, *Tellus*, Vol. 56A, pp. 415-428,

2004.

- Palmer, P. I., Jacob, D. J., Jones, D. B. A., Heald, C. L., Yantosca, R. M., Logan, J. A., Sachse, G. W. and Streets, D. G.:
690 Observations over the western Pacific, 2003.
- Parrington, M., Jones, D. B. A., Bowman, K. W., Horowitz, L. W., Thompson, A. M., Tarasick, D. W. and Witte,
J. C.: Estimating the summertime tropospheric ozone distribution over North America through assimilation of
observations from the Tropospheric Emission Spectrometer, *Journal of Geophysical Research*, Vol 113, D18307,
doi:10.1029/2007JD009341, 2008.
- 695 Parrington, M., Jones, D. B. A., Bowman, K. W., Thompson, A. M., Tarasick, D. W., Merrill, J., Oltmans, S. J., Leblanc,
T., Witte, J. C. and Millet, D. B.: Impact of the assimilation of ozone from the tropospheric emission spectrometer
on surface ozone across North America, *Geophysical Research Letters* 36 (4), 2009.
- Parrish, D. F. and Derber, J. C.: The national meteorological center's spectral statistical-interpolation analysis system,
Monthly Weather Review, (120), p. 1747–1763, 1992.
- 700 Pierce, R. B., et al.: Chemical data assimilation estimates of continental U. S. ozone and nitrogen budgets
during the Intercontinental Chemical Transport Experiment-North America, *J. Geophys. Res.*, 112, D12S21,
doi:10.1029/2006JD007722, 2007.
- R. B. Pierce, J. Al-Saadi, C. Kittaka, T. Schaack, A. Lenzen, K. Bowman, J. Szykman, A. Soja, T. Ryerson, A. M.
Thompson, P. Bhartia, and G. A. Morris. Impacts of background ozone production on Houston and Dallas, Texas,
705 air quality during the Second Texas Air Quality Study field mission. *J. Geophys. Res.*, 114, 05 2009.
- Pires, C., Vautard, R., and Talagrand, O.: On extending the limits of variational assimilation in nonlinear chaotic
systems, *Tellus*, 48A, 960-121, 1996.
- Price, C., and Rind, D.: A Simple Lightning Parameterization for Calculating Global Lightning Distributions, *J. Geo-
phys. Res.*, 97(D9), 9919–9933, doi:10.1029/92JD00719, 1992.
- 710 Rabier, F., Jarvinen, H., Klinker, E., Mahfouf, J. -F. and Simmons, A.: The ECMWF operational implementation of
four-dimensional variational data assimilation I: Experimental results with simplified physics, *Quarterly Journal of
the Royal Meteorological Society*, 126:1143–1170, 2000.
- Sandu, A., Daescu, D., and Carmichael, G.R.: Direct and Adjoint Sensitivity Analysis of Chemical Kinetic Systems
with KPP: I - Theory and Software Tools, *Atmos. Environ.*, 37(36):5083-5096, 2003.
- 715 Daescu D.N., Sandu A., Carmichael G.R.: Direct and adjoint sensitivity analysis of chemical kinetic systems with KPP:
II - Numerical validation and applications, *Atmos. Environ.*, 37(36):5097–5114, 2003.
- Sandu, A., Daescu, D. N., Carmichael, G. R. and Chai, T.: Adjoint sensitivity analysis of regional air quality models,
Journal of Computational Physics, Vol. 204, p. 222–252, 2005.
- Sandu A., Liao W., Carmichael G.R., et al.: Inverse modeling of aerosol dynamics using adjoints: Theoretical and
720 numerical considerations, *Aerosol science and Technology*, 39(8):677–694, 2005.
- Sandu A. and Zhang L.: Discrete second order adjoints in atmospheric chemical transport modeling, *Journal of
Computational Physics*, 227 (12), 5949–5983, 2008.
- Sasaki, Y. K.: An objective analysis based on the variational method, *J. Met. Soc. Jap.* II(36), 77–88, 1958.
- Segers, A. J., Eskes, H. J., van der A, R. J., van Oss, R. F. and van Velthoven, P. F. J.: Assimilation of GOME ozone
725 profiles and a global chemistry-transport model, using a Kalman Filter with anisotropic covariance, *Quarterly
Journal of the Royal Meteorological Society*, 131, 477-502, 2005.
- Singh, K., Eller, P., Sandu, A., Bowman, K. W., Jones, D. B. A. and Lee, M.: Improving GEOS-Chem model forecasts

- through profile retrievals from Tropospheric Emission Spectrometer, in: Lecture Notes on Computational Science vol. 5545, p. 302–311, International Conference on Computational Science 2009, Baton Rouge, Louisiana, May 25–27, 2009.
- 730 Singh, K., Eller, P., Sandu, A., Henze, D., Bowman, K. W., Kopacz, M. and Lee, M.: Towards the construction of a standard adjoint GEOS-Chem model, High Performance Computing Symposium (HPC 2009) at Spring Simulation Multiconference (SpringSim'09), San Diego, California, March 22–27, 2009.
- 735 Singh, K., Jardak, M., Sandu, A., Bowman, K. W., Jones, D. B. A., Lee, M.: Construction of non-diagonal background error covariance matrices in global chemical data assimilation, *Geophysical Model Development*, 4, 299–316, doi:10.5194/gmd-4-299-2011, 2011.
- Singh, K., Sandu, A., Jardak, M., Bowman, K. W., Lee, M.: A Practical Method to Estimate Information Content in the Context of 4D-VAR Data Assimilation, *to be submitted to Journal of Geophysical Research*, 2011.
- 740 Singh, K., Sandu, A.: Variational Chemical Data Assimilation with Approximate Adjoint, *accepted in Computers & Geosciences-Elsevier*, 2011.
- Stevenson, D. S., et al.: Multimodel ensemble simulations of present-day and near-future tropospheric ozone, *J. Geophys. Res.*, 111, D08301, doi:10.1029/2005JD006338, 2006.
- Tang YH, Carmichael GR, Horowitz LW, A. Sandu, et. al: Multiscale simulations of tropospheric chemistry in the Eastern Pacific and on the US West Coast during spring 2002 *Journal of Geophysical Research-Atmospheres*, Volume: 745 109, Issue: D23, Article Number: D23S11, 2004.
- Tarasick, D. W., Fioletov, V. E., Wardle, D. I., Kerr, J. B., and Davies, J.: Changes in the vertical distribution of ozone over Canada from ozonesondes: 1980–2001, *J. Geophys. Res.*, 110, D02304, doi:10.1029/2004JD004643, 2005.
- Tellmann, S., Rozanov, V. V., Weber, M., and Burrows, J. P.: Improvements in the tropical ozone profile retrieval from GOME-UV/Vis nadir spectra, *Adv. Space Res.*, 34(4), 739–743, 2004.
- 750 TES Science Team, TES L2 Data Users Guide, Jet Propulsion Laboratory, California Institute of Technology, Pasadena, California. (Available at <http://tes.jpl.nasa.gov/docsLinks/DOCUMENTS/TESL2DataUsersGuidev2.0.pdf>), 2006.
- Thompson, A. M., et al.(2007a): Intercontinental chemical transport experiment ozonesonde network study (IONS) 2004: 1. Summertime upper troposphere/lower stratosphere ozone over northeastern North America, *J. Geophys. Res.*, 112 D12S12, doi:10.1029/2006JD007441, 2007. Thompson, A. M., et al.(2007b): Intercontinental chemical transport experiment ozonesonde network study (IONS) 2004: 2. Tropospheric ozone budgets and variability over northeastern North America, *J. Geophys. Res.*, 112 D12S13, doi:10.1029/2004JD005359, 2007.
- 755 Todling, R., Cohn, S. E.: Suboptimal Schemes for Atmospheric Data Assimilation Based on the Kalman Filter, *Monthly Weather Review*, 122, 2530–2557, 1994.
- Worden, J. R., Bowman, K. W. and Jones, D. B. A.: Characterization of atmospheric profile retrievals from Limb Sounding Observations of an inhomogeneous atmosphere, *J. Quant. Spectrosc. Radiat. Transfer*, 86, (03)00274–7, 760 2004.
- Wu, L., Mallet, V., Bocquet, M. and Sportisse, B.: A comparison study of data assimilation algorithms for ozone forecasts, *J. Geophys. Res.*, 113, D20310, 2008.
- Yevich, R., and Logan, J. A.: An assessment of biofuel use and burning of agricultural waste in the developing world, *Global Biogeochem. Cycles*, 17(4), 1095, doi:10.1029/2002GB001952, 2003.
- 765 Zhang, L., Constantinescu, E. M., Sandu, A., Tang, Y., Chai, T., Carmichael, G. R., Byun, D., Olaguer, E.: An adjoint sensitivity analysis and 4D-Var data assimilation study of Texas air quality, *Atmospheric Environment*, Vol. 42,

Issue 23, p. 5787–5804, 2008.

Zhang, L., Jacob, D. J., Kopacz, M., Henze, D. K., Singh, K., and Jaffe, D. A.: Intercontinental source attribution of ozone pollution at western U.S. sites using an adjoint method, *Geophys. Res. Lett.*, 36, L11810, doi:10.1029/2009GL037950, 2009.

Zhu, C., Byrd, R. H. and Nocedal, J.: L-BFGS-B: Algorithm 778: L-BFGS-B, FORTRAN routines for large scale bound constrained optimization, *ACM Transactions on Mathematical Software*, Vol 23, Num. 4, pp. 550 - 560, 1997.

Appendix A The 3D-Var equivalent initial condition

Finally, we want to determine the “3D-Var equivalent initial condition” $\mathbf{x}_0^{e(3)}$ such that the resulting trajectory fits best the 3D-Var analysis in a least squares sense. To our knowledge, no attempt has been made to date to estimate the equivalent effect of all 3D-Var corrections at the initial time. (Note that the 3D-Var analysis is not a trajectory of the model). The dynamic equations for the 3D-Var trajectory, linearized about the 4D-Var analysis, read:

$$\mathbf{x}_i^{a(3)} - \mathbf{x}_i^{a(4)} = \mathbf{M}_i \cdot \left(\mathbf{x}_0^{e(3)} - \mathbf{x}_0^{a(4)} \right) + \theta_i, \quad i = 0, \dots, N. \quad (\text{A1})$$

The errors $\theta_i = \mathbf{x}_i^{a(3)} - \mathbf{x}_i^{a(4)}$ are assumed to be normally distributed with mean zero and covariance \mathbf{Q}_i . We now seek the equivalent 3D-Var initial condition that solves (A1) in a least squares sense. The scaled linearized dynamic equations are

$$\mathbf{Q}_i^{-1/2} \mathbf{M}_i \left(\mathbf{x}_0^{e(3)} - \mathbf{x}_0^{a(4)} \right) - \mathbf{Q}_i^{-1/2} \left(\mathbf{x}_i^{a(3)} - \mathbf{x}_i^{a(4)} \right) = \mathbf{Q}_i^{-1/2} \theta_i, \quad i = 0, \dots, N,$$

and involve the scaled residuals $\mathbf{Q}_i^{-1/2} \theta_i$ which are standard normal random vectors. Therefore the least squares solution is the one that minimizes the sum of scaled residual norms squared

$$\mathbf{x}_0^{e(3)} = \arg \min \sum_{i=0}^N \left\| \mathbf{M}_i \left(\mathbf{x}_0^{e(3)} - \mathbf{x}_0^{a(4)} \right) - \left(\mathbf{x}_i^{a(3)} - \mathbf{x}_i^{a(4)} \right) \right\|_{\mathbf{Q}_i^{-1}}^2.$$

The minimum of this quadratic function is obtained by imposing that its gradient equals zero. This leads to the following system of linear equations:

$$\underbrace{\left(\sum_{i=0}^N \mathbf{M}_i^T \mathbf{Q}_i^{-1} \mathbf{M}_i \right)}_{\nabla_{\mathbf{x}_0^a, \mathbf{x}_0^a}^2 \mathcal{D}(\mathbf{x}_0^{a(4)})} \left(\mathbf{x}_0^{e(3)} - \mathbf{x}_0^{a(4)} \right) = \underbrace{\sum_{i=0}^N \mathbf{M}_i^T \mathbf{Q}_i^{-1} \left(\mathbf{x}_i^{a(3)} - \mathbf{x}_i^{a(4)} \right)}_{\nabla_{\mathbf{x}_0^a} \mathcal{D}(\mathbf{x}_0^{a(4)})}.$$

Therefore the least squares solution to finding the 3D-Var equivalent initial condition is

$$\mathbf{x}_0^{e(3)} = \mathbf{x}_0^{a(4)} - \left(\nabla_{\mathbf{x}_0^a, \mathbf{x}_0^a}^2 \mathcal{D}(\mathbf{x}_0^{a(4)}) \right)^{-1} \cdot \nabla_{\mathbf{x}_0^a} \mathcal{D}(\mathbf{x}_0^{a(4)}). \quad (\text{A2})$$

Consider a standard normal random perturbation is applied at t_0 to the 4D-Var optimal initial condition. This perturbation is propagated through the linearized model, and its covariance at t_i is $\mathbf{M}_i \mathbf{M}_i^T$. Let

$\mathbf{Q}_i = \rho_i \mathbf{M}_i \mathbf{M}_i^T$ in (23) in order to account for an increasing error with the model evolution. The scalar weights ρ_i decrease with i , to account for the reduction in uncertainty through 3D-Var assimilation, and are chosen such that $\sum_{i=0}^N \rho_i = 1$. Using the fact that $\mathbf{M}_i^T \mathbf{Q}_i^{-1} \mathbf{M}_i = \mathbb{I}$ for all i we have that the equivalent 3D-Var initial solution is

$$\mathbf{x}_0^{e(3)} = \mathbf{x}_0^{a(4)} - \sum_{k=0}^N \mathbf{M}_k^T \mathbf{Q}_k^{-1} (\mathbf{x}_0^{a(4)} - \mathbf{x}_0^{a(3)}) = \mathbf{x}_0^{a(4)} - \nabla_{\mathbf{x}_0^a} \mathcal{D}(\mathbf{x}_0^{a(4)}).$$

The 3D-Var solution has incorporated all the observation information when it reaches t_N , the end of the assimilation window. Therefore it makes sense to choose $\rho_0 = \dots = \rho_{N-1} = 0$ and $\rho_N = 1$ in order to have the equivalent initial condition match the 3D-Var analysis only at the final time. In this case

$$\mathbf{x}_0^{e(3)} = \mathbf{x}_0^{a(4)} - \left(\mathbf{M}_N^T \mathbf{Q}_N^{-1} \mathbf{M}_N \right)^{-1} \mathbf{M}_N^T \mathbf{Q}_N^{-1} (\mathbf{x}_0^{a(4)} - \mathbf{x}_0^{a(3)}). \quad (\text{A3})$$